HHS Public Access

Author manuscript

Cell. Author manuscript; available in PMC 2025 January 18.

Published in final edited form as:

Cell. 2024 January 18; 187(2): 294–311.e21. doi:10.1016/j.cell.2023.11.022.

Metabolic regulation of homologous recombination repair by MRE11 lactylation

Yuping Chen[1,2,14], **Jinhuan Wu**[1,2,14], **Linhui Zhai**[3,13], **Tingting Zhang**[4], **Hui Yin**[5], **Huanyao Gao**[6], **Fei Zhao**[7], **Zhe Wang**[1,2], **Xiaoning Yang**[8], **Mingpeng Jin**[1,2], **Bingsong Huang**[1,2], **Xin Ding**[1,2], **Rui Li**[1,2], **Jie Yang**[9], **Yiming He**[1,2], **Qianwen Wang**[1,2], **Weibin Wang**[10], **Jake A. Kloeber**[7,11], **Yunxuan Li**[4], **Bingbing Hao**[3,13], **Yuanyuan Zhang**[1], **Jiadong Wang**[10], **Minjia Tan**[3,13], **Ke Li**[4], **Ping Wang**[12], **Zhenkun Lou**[6,7], **Jian Yuan**[1,2,15,*]

[1]State Key Laboratory of Cardiology and Research Center for Translational Medicine, Shanghai East Hospital, Tongji University School of Medicine, Shanghai 200120, China

[2]Department of Biochemistry and Molecular Biology, Tongji University School of Medicine, Shanghai 200120, China

[3]State Key Laboratory of Drug Research, Shanghai Institute of Materia Medica, Chinese Academy of Sciences, Shanghai 201203, China

[4]Institute of Medicinal Biotechnology, Chinese Academy of Medical Sciences & Peking Union Medical College, Beijing 100050, China

[5]Department of Thoracic Surgery, The First Affiliated Hospital of Shaoyang University, Shaoyang 422001, China

[6]Department of Molecular Pharmacology and Experimental Therapeutics, Mayo Clinic, Rochester, MN 55905, USA

[7]Department of Oncology, Mayo Clinic, Rochester, MN 55905, USA

[8]Institute of Materia Medica, Chinese Academy of Medical Sciences & Peking Union Medical College, Beijing 100050, China

[9]Department of Thoracic Surgery, The First Affiliated Hospital of Nanchang University, Nanchang 330006, China

[10]Department of Radiation Medicine, School of Basic Medical Sciences, Peking University Health Science Center, Beijing 100191, China

[*]Correspondence: yuanjian229@hotmail.com.

AUTHOR CONTRIBUTIONS

J. Yuan and Y.C. conceived the project and designed the studies. Y.C. and J. Wu conducted the experiments. Y.C. wrote the paper. J. Yuan, Z.L., and J.A.K. revised the manuscript. M.T., L.Z., and B. Hao performed the MS. K.L. and T.Z. conducted the mouse drug toxicology experiment of K673-pe peptides. H.G. conducted bioinformatics data. H.Y., F.Z., Z.W., X.Y., M.J., B. Huang, X.D., R.L., J. Yang, Y.H., Q.W., W.W., Y.L., Y.Z., J. Wang, and P.W. provided the constructional suggestions and help for this paper.

DECLARATION OF INTERESTS

The authors declare no competing interests.

INCLUSION AND DIVERSITY

We support inclusive, diverse, and equitable conduct of research.

SUPPLEMENTAL INFORMATION

Supplemental information can be found online at https://doi.org/10.1016/j.cell.2023.11.022.

[11]Mayo Clinic Medical Scientist Training Program, Mayo Clinic Alix School of Medicine and Mayo Clinic Graduate School of Biomedical Sciences, Mayo Clinic, Rochester, MN 55905, USA

[12]Tongji University Cancer Center, Shanghai Tenth People's Hospital, School of Medicine, Shanghai 200072, China

[13]University of Chinese Academy of Sciences, Beijing, China

[14]These authors contributed equally

[15]Lead contact

SUMMARY

Lactylation is a lactate-induced post-translational modification best known for its roles in epigenetic regulation. Herein, we demonstrate that MRE11, a crucial homologous recombination (HR) protein, is lactylated at K673 by the CBP acetyltransferase in response to DNA damage and dependent on ATM phosphorylation of the latter. MRE11 lactylation promotes its binding to DNA, facilitating DNA end resection and HR. Inhibition of CBP or LDH downregulated MRE11 lactylation, impaired HR, and enhanced chemosensitivity of tumor cells in patient-derived xenograft and organoid models. A cell-penetrating peptide that specifically blocks MRE11 lactylation inhibited HR and sensitized cancer cells to cisplatin and PARPi. These findings unveil lactylation as a key regulator of HR, providing fresh insights into the ways in which cellular metabolism is linked to DSB repair. They also imply that the Warburg effect can confer chemoresistance through enhancing HR and suggest a potential therapeutic strategy of targeting MRE11 lactylation to mitigate the effects.

In brief

Lactate-induced MRE11 lactylation in cancer cells leads to HR hyperactivation and chemoresistance. The findings unveil new insights into the ways in which cellular metabolism is tied to DSB repair and the impact of the Warburg effect on chemoresistance.

Graphical abstract

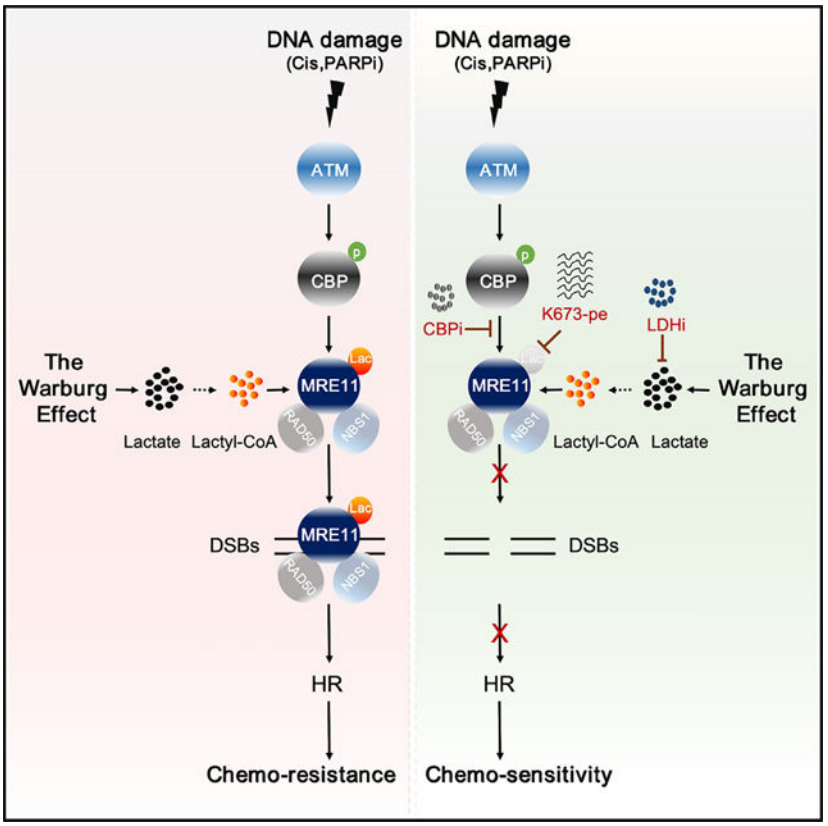

INTRODUCTION

The Warburg effect, also known as aerobic glycolysis, is a metabolic hallmark of most cancers. It involves a process where large volumes of lactate are produced, despite the presence of oxygen in cancer cells.[1–3] The intermediate metabolite lactate is derived from pyruvate in a reaction catalyzed by lactate dehydrogenase (LDH) in cancer cells and is known to play key roles in various cellular processes, which promote tumor cell proliferation, metastatic dissemination, and immune suppression.[4,5] However, its non-metabolic functions in cancer cells remain largely unknown. Recently, Zhang and colleagues reported that in addition to its metabolic functions, lactate also induces a previously unknown post-translational modification (PTM) called lactylation and that lactylation of histone lysine residues functions as an epigenetic modification that regulates gene transcription.[6] However, it remains largely unclear what the functions of lactylation are in proteins.

The maintenance of genomic integrity is vital for ensuring the faithful transmission of genetic materials across generations.[7,8] Endogenous and exogenous DNA damage and errors in DNA replication are major sources of genomic instability.[9] Double-strand breaks (DSBs) are the most deleterious forms of DNA lesions and pose great threats to genome instability. DSB repair defects have been implicated in several diseases, including cancer, neurological disorders, growth retardation, and immune deficiency.[10–13] The current model suggests that there are two main pathways responsible for repairing DSBs as follows:

non-homologous end-joining (NHEJ) and homologous recombination (HR).[14,15] NHEJ directly conjugates the broken ends together, meaning it is quicker than HR but is error-prone and may introduce a large number of mutations.[16] Unlike NHEJ, which happens across the entire cell cycle, HR primarily occurs during S and G2 phases because of its requirement for a homologous template.[17] As a result, HR is an error-free mechanism for DSBs repair. One of the key initial steps in HR is the end resection of damaged DNA, which generates proper single-strand DNA.[18] In mammals, end resection is initiated by the MRE11 (meiotic recombination 11)/RAD50/NBS1 (Nijmegen breakage syndrome 1) (MRN) complex and then promoted by phosphorylated forms of CtIP (CtBP [C-terminal binding protein] interacting protein).[19–21] The MRN complex is a versatile complex, playing a key role in the sensing, processing, and repair of DSBs.[22–24]

MRE11, the core component of the MRN complex, possesses both endonuclease and $3'-5'$ exonuclease activity.[23,25] MRE11 contains two DNA-binding domains (DBDs), enabling it to bind both single-stranded DNA (ssDNA) and double-stranded DNA (dsDNA). After DSBs, MRE11 is loaded onto DSBs sites and cleaves DNA by cooperating with CtIP to initiate end resection. Long-range extensive DNA resection is subsequently completed by exonucleases EXO1 and DNA2. The resulting ssDNA is rapidly coated and protected by replication protein A (RPA), which is then replaced by the RAD51 recombinase to form a nucleofilament that is vital for the generation of homology and the subsequent steps of the HR process.[26,27] Accumulating studies have indicated that overactivation of HR is a major driver of chemoresistance in cancers.[28–30] Metabolic abnormalities are some of the most prominent characteristics of cancer cells. The best-known metabolic alteration in cancer cells is the Warburg effect, which is defined by a significant increase in glycolysis even in the case of sufficient oxygen.[31] However, it is unknown whether HR is regulated by the Warburg effect.

Herein, we demonstrate that lactylation regulates HR. Mechanistically, MRE11 is lactylated following DNA damage. CBP catalyzes MRE11 lactylation at K673, which is located in its second DBD. MRE11 lactylation exerts a key function in regulating MRE11 DNA-binding ability and subsequent DNA end resection. High MRE11 lactylation promotes HR and chemoresistance in cancer cells. In addition, we designed a cell-penetrating peptide (CPP) to target lactylation of MRE11 K673. This peptide presents evident inhibition of MRE11 K673 lactylation and impairs HR, which in turn promotes cancer cell sensitivity to chemotherapy. Taken together, our findings indicate that MRE11 lactylation promotes HR, and targeting MRE11 lactylation might be an effective strategy to overcome chemoresistance in cancers.

RESULTS

Lactylation promotes DNA damage repair and chemoresistance

As lactylation is a recently identified PTM, its role in cells remains largely unknown. LDHA is a major enzyme mediating lactate production,[32] which may in turn promote protein lactylation.[6] Intriguingly, we found that patients with low *LDHA* expression levels showed higher HR deficiency (HRD) scores (an indicator of HRD), suggesting that high levels of lactate or protein lactylation might exert a pivotal function in HR repair (Figure 1A). To test this hypothesis and separate the roles of lactate and protein lactylation, we treated cells

with sodium lactate (NALA), which induced a high degree of protein lactylation but did not affect cellular lactate levels (Figures 1B and S1A), and examined them with an HR reporter assay. As shown in Figures 1B and 1C, NALA treatment increased pan-lactylation in cells (Figure 1B) and enhanced HR repair (Figure 1C). In addition, NALA decreased irradiation (IR)-induced γ-H2AX foci at later time points (8 and 24 h), suggesting that NALA treatment facilitated DNA damage repair (Figures 1D and 1E). Therefore, an LDH inhibitor (LDHi) decreased lactate levels (Figure S1B) and pan-lactylation (Figure 1F) and inhibited HR (Figure 1G). Furthermore, LDHi treatment resulted in strong γ-H2AX foci at later time points (8 and 24 h), suggesting that LDHi impaired DNA damage repair (Figures 1H and 1I). Notably, neither NALA nor LDHi treatment had obvious effects on the cell cycle (Figure S1C). Previous studies have suggested that HRD renders cancer cells sensitive to platinum or PARP (poly [ADP-ribose] polymerase) inhibitor (PARPi) treatment. Thus, we next examined whether manipulating lactylation in cancer cells would affect their responses to chemotherapy. As shown in Figures 1J–1L, NALA treatment increased protein lactylation and led cells to become resistant to cisplatin or olaparib treatment. By contrast, LDHi treatment decreased protein lactylation and sensitized cancer cells to cisplatin, olaparib, or etoposide (Figures 1M–1P). In addition, depletion of *LDHA/B*, which resulted in a significant reduction of lactate in cells, also markedly sensitized cancer cells to olaparib (Figures 1Q, 1R, and S1D).

Given that lactate could promote DNA repair by inducing expression (or transcriptional expression) of DNA damage-related genes,[33] we wondered whether NALA also controlled DNA repair in a transcription-dependent manner. As shown in Figures S1E–S1G, unlike lactate treatment, NALA treatment did not affect the levels of acetylated histone H3 and H4 (acetyl-H3 and acetyl-H4), which were reported to regulate DSB repair,[33] and did not affect the transcription of several key DNA repair genes, especially those involved in DSB repair. Additionally, although both NALA and lactate promoted DNA end resection, HR repair efficiency, and cancer cell survival after chemotherapy, lactate had a relatively greater effect (Figures S1H–S1K). All these data indicated that NALA might regulate DNA repair in a transcription-independent manner. Taken together, these results suggest that protein lactylation may play a key role in DNA damage repair.

MRE11 is lactylated by CBP acetyltransferase

After screening several key HR proteins, we found that MRE11 was strongly lactylated in cells (Figure 2A). NALA treatment enhanced the MRE11 lactylation, and LDHi treatment had the opposite effect (Figure 2B). Depletion of *LDHA/B* remarkedly decreased MRE11 lactylation (Figure 2C). Additionally, MCT1/4 inhibitor (MCT1/4i) treatment, which elevated cellular lactate levels, also remarkedly increased the MRE11 lactylation (Figures S2A and S2B). Interestingly, MRE11 lactylation was also increased by several DNA-damaging agents (Figure 2D).

Since previous studies have reported that lactylation occurs in both enzymatic- and non-enzymatic-dependent manners,[6,34] we next examined the underlying mechanism of MRE11 lactylation. As shown in Figures S2C and S2D, inhibition or depletion of *GLO1*, a key regulator of non-enzymatic lactylation, did not affect MRE11 lactylation. However, after

screening multiple acetyltransferases, we found that CBP primarily mediated MRE11 lactylation (Figure 2E). Depletion of *CBP* or CBP inhibition sharply decreased MRE11 lactylation (Figures 2F and 2G). We also found that CBP bound to MRE11 (Figures 2H and S2E). The interaction between MRE11 and CBP was obviously increased following cisplatin treatment (Figures 2I and S2F). However, treatment with an ATM (ataxia-telangiectasia mutated) inhibitor was able to inhibit MRE11-CBP binding (Figures 2I and S2F) and DNA damage-induced MRE11 lactylation (Figure 2G). Meanwhile, we also found that CBP was phosphorylated by ATM after DNA damage using a p-SQ/TQ(ATM/ATR phosphorylate serine [S] or threonine [T] residues with glutamine [Q] at the +1 position [the so-called SQ/TQ motif]) substrate antibody, and this phosphorylation was abolished by ATM inhibitor treatment (Figure S2G). In addition, we found that CBP S124 was the major site of ATM-mediated phosphorylation following DNA damage (Figure S2H). Mutating this site in *CBP* (*S124A*) decreased the interaction between CBP and MRE11 (Figure S2I), suggesting that the ATM-mediated phosphorylation of CBP was important for its binding to MRE11. Hence, our findings suggest that ATM may promote the interaction between CBP and MRE11 by mediating CBP phosphorylation, which then enhances CBP-mediated MRE11 lactylation. Furthermore, CBP-mediated MRE11 lactylation was confirmed with an *in vitro* lactylation assay (Figures 2J and S2J). Since nicotinamide (NAM), a sirtuin family inhibitor, markedly increased MRE11 lactylation (Figures S2K and S2L), we also explored potential “eraser(s)” of MRE11 lactylation by screening sirtuin family members. Our results suggested that SIRT1 (sirtuin 1) and SIRT2 (sirtuin 2) were two major regulators of MRE11 delactylation (Figure S2M).

MRE11 is lactylated at K673

MRE11 is an evolutionarily conserved protein that mainly consists of a nuclease domain, two DBDs, and a GAR (glycine arginine rich) domain (Figure 2K). To identify potential MRE11 lactylation sites, we performed mass spectrometry (MS). As shown in Figures 2K, 2L, and S2N–S2P, four sites (K510, K609, K625, and K673) were identified as possible MRE11 lactylation sites. However, K673, which is located in the second DBD, was found to be the main lactylation site in response to DNA damage (Figures 2M and S2Q). The MRE11 K673 site is highly conserved across different species (Figure S2R). To facilitate the specific recognition of MRE11 K673 lactylation, an antibody was generated (hereafter referred to as MRE11-K673la). We found that lactylation at MRE11 K673 was significantly increased in response to DNA damage and that the MRE11 K673R mutant abolished the signal detected by the MRE11-K673la antibody (Figure 2N). MCT1/4i treatment also remarkedly enhanced the lactylation of MRE11 K673 (Figure S2S). Additionally, overexpression of *CBP* significantly increased lactylation of MRE11 wild type (WT) but not the MRE11 K673R mutant (Figure 2O). By contrast, depletion of *CBP* sharply decreased K673 lactylation of MRE11 WT but not of the MRE11 K673R mutant (Figure S2T). To further confirm the MRE11 lactylation sites, we performed an *in vitro* lactylation assay using purified GST (glutathione S-transferase) fusion MRE11 WT and K673R mutant proteins. As shown in Figures 2P and S2U, GST-MRE11 WT, but not the K673R mutant, was lactylated *in vitro*. Taken together, our results suggest that K673 is the main site of CBP-meditated MRE11 lactylation in response to DNA damage.

MRE11 lactylation enhances its DNA-binding ability

MRE11 has two DBDs and has been reported to bind DNA in RAD50-dependent and -independent manners.[23,35–39] However, the mechanism underlying MRE11 DNA binding is still very unclear. Thus, we examined whether MRE11 lactylation affected its binding to DNA. First, we found that MRE11 lactylation did not affect complex formation between MRE11, RAD50, and NBS (Figures 3A and S3A). To examine whether lactylation played a role in MRE11 DNA binding, purified MRE11 WT was first utilized to perform *in vitro* lactylation assays and then *in vitro* DNA-binding assays. As shown in Figures 3B–3D, S3B, and S3C, electrophoretic mobility shift assay (EMSA) results suggested that MRE11 lactylation facilitated MRE11 or MR (RAD50 and MRE11 complex) binding to dsDNA and overhang DNA. Additionally, compared with the MRE11 K673R mutant, MRE11 WT had a higher affinity for binding DNA (Figures 3E, 3F, and S3D). Furthermore, NALA treatment enhanced MRE11 and MRE11-K673la foci formation and MRE11 chromatin loading (Figures 3G–3J and S3E–S3G). Additionally, MRE11 foci formation and chromatin recruitment were decreased by the inhibition or depletion of *CBP* or LDHi treatment (Figures 3G–3L and S3E–S3H). Furthermore, protein retention of MRE11 K673R in the chromatin fraction was dramatically decreased compared with MRE11 WT (Figures 3I, 3J, and S3E–S3G). Similarly, MRE11 K673R showed decreased foci formation following DNA damage (Figures 3M and S3I). In addition, we found that, compared with the soluble fractions, lactylated MRE11 was enriched in chromatin-bound fractions after DNA damage (Figure S3J). Meanwhile, we conducted a semi-quantification analysis based on the MS extracted ion chromatogram (XIC) and found that the lactylation percentage of K673 was calculated to be about 0.50% based on total MRE11 levels (Figure S3K). As previous studies have shown that the phosphorylation status of MRE11 S676 and S678 is important for MRE11 DNA binding and repair,[40,41] we next determined whether lactylation of MRE11 K673 regulated MRE11 DNA binding by affecting the phosphorylation of MRE11 S676 and S678. As shown in Figures S3L and S3M, there was no mutual impact between the lactylation of MRE11 K673 and the phosphorylation of MRE11 S676/S678. Taken together, our findings suggest that lactylation of MRE11 is important for its DNA-binding ability and foci formation.

MRE11 lactylation enhances end resection

To further explore whether lactylation affected DNA end resection, cells treated with NALA or LDHi were employed to examine phospho-RPA2 (replication protein A2) and 5-bromo-2′-deoxyuridine (BrdU) foci formation. Both LDHi treatment and depletion of *LDHA/B* markedly decreased cisplatin-induced phospho-RPA2 levels (Figures 4A, 4B, and S3N). However, NALA treatment was able to rescue the phospho-RPA2 levels impaired by the depletion of *LDHA/B* or LDHi treatment (Figures 4A and 4B), but not those impaired by the depletion of *CBP* or *MRE11* (Figures S3O and S3P). In addition, the overexpression of *CBP* in control cells, but not in *MRE11*-depleted cells, obviously increased the levels of phospho-RPA2 (Figure S3Q). These findings suggest that lactylation may regulate DNA end resection via the CBP-MRE11 axis.

Next, we found that NALA treatment markedly increased RPA2, BrdU, and RAD51 foci formation after DNA damage (Figures 4C–4E). However, LDHi inhibited RPA2, BrdU,

and RAD51 foci formation (Figures 4C–4E). To further explore the role of MRE11 K673 lactylation in DNA end resection, we constructed stably expressing *MRE11 WT* or *MRE11 K673R* cancer cells where endogenous *MRE11* was depleted (Figure S3R). We found that *MRE11 K673R* cells inhibited phospho-RPA2 levels after DNA lesions (Figure 4F). In addition, NALA increased phospho-RPA2 levels in cells expressing *MRE11 WT* but not in *MRE11 K673R* mutant cells, following DNA damage (Figure 4F). Furthermore, *MRE11 K673R* mutants impaired RPA2, BrdU, and RAD51 foci formation following DNA damage (Figures 4G–4I). We also further confirmed the role of MRE11 lactylation in DNA end resection using a qPCR-based DNA resection measurement system.[42] We found that *MRE11 K673R* mutant cells markedly reduced ssDNA formation compared with *MRE11 WT* cells (Figures 4J and 4K). Next, as it has been reported that MRE11 K673 may be able to be ubiquitinylated,[43,44] we wondered whether mutating MRE11 K673 affected its ubiquitination or stability. As shown in Figures S3S and S3T, the K673R mutation did not affect MRE11 ubiquitination or stability. Taken together, our findings suggest that CBP-mediated MRE11 lactylation may be vital for DNA resection following DSBs.

Next, to rule out the possibility that K673 was also a CBP-mediated acetylation site at MRE11, which in turn regulates DNA end resection and HR repair, we performed a series of experiments to clarify the roles of lactylation and acetylation in MRE11 functional regulation. As shown in Figure S4A, we found that MRE11 was acetylated by a pan-acetylation antibody. However, the mutation of MRE11 K673R did not affect MRE11 pan-acetylation levels (Figure S4A). Next, we screened the writer(s) for MRE11 acetylation. Unlike the writer for lactylation of MRE11, the major writer for acetylation of MRE11 is GCN5 (general control non-depressible 5) (Figure S4B). Overexpression of *GCN5* markedly increased MRE11 acetylation levels, and depletion of *GCN5* markedly decreased MRE11 acetylation levels (Figures S4C and S4D). However, overexpression or knockdown of *GCN5* did not affect MRE11 lactylation (Figures S4C and S4D). In addition, overexpression or depletion of *CBP* affected MRE11 lactylation but not acetylation (Figures S4E and S4F). Moreover, our findings indicated that CBP only catalyzed lactylation but not MRE11 acetylation, and GCN5 only catalyzed acetylation but not MRE11 lactylation *in vitro* (Figures S4G and S4H).

To further detect whether K673 was an acetylation site on MRE11, we also generated an anti-MRE11-K673 acetylation-specific antibody (termed as MRE11-K673ac). As shown in Figures S4A and S4C–S4H, we did not detect any signal of MRE11 K673 acetylation *in vivo* or *in vitro by* using this antibody, although the antibody had good specificity and showed a strong signal in dot blot assays (Figure S4A). Thus, these results suggest that MRE11 is acetylated and that the acetyltransferase is GCN5, but that K673 is not a site of MRE11 acetylation.

Next, we determined whether *GCN5* regulated DNA end resection. As shown in Figures S3O and S4I–S4K, unlike *CBP*, overexpression or depletion of *GCN5* had no effect on the levels of phospho-RPA2. Additionally, we found that NALA could induce MRE11 K673 lactylation and DNA end resection (Figures S4L and S4M). However, NAAC (sodium acetate) was able to induce MRE11 acetylation but had no obvious effects on DNA end resection (Figures S4L and S4M).

To further identify MRE11 acetylation sites, we performed MS using purified MRE11 proteins. From the MS results, we found several possible sites of MRE11 acetylation (Figures S4N–S4S). Further assays determined that K609 was the major site of MRE11 acetylation in response to DNA damage (Figure S5A). In addition, our results indicated that K609 was the major site of GCN5-mediated MRE11 acetylation *in vitro* (Figure S5B). Next, we confirmed that MRE11 K673 lactylation, but not K609 acetylation, was important for DNA end resection and HR repair (Figures S5C and S5D).

In summary, our findings demonstrate different roles for MRE11 lactylation and acetylation. These two modifications appear to be functionally discrete, with separate modification sites and writers, and have no crosstalk on MRE11 activity. Only K673 lactylation, but not K609 acetylation, was found to facilitate DNA end resection and HR repair. Thus, our findings suggest that lactylation, but not MRE11 acetylation, facilitates DNA end resection and HR repair.

Lactylation of MRE11 promotes HR

Since lactylation of MRE11 enhanced DNA resection, which is a key step in HR repair, we next tested whether the MRE11 lactylation regulated HR repair and/or genomic stability. As shown in Figures 5A, S5E, and S5F, M*RE11 K673R* mutants decreased HR repair but did not clearly affect the transcriptional expression of several key DNA repair, particularly DSB repair, related genes (Figure S5G). Furthermore, the *MRE11 K673R* mutant impaired DNA damage repair, which was identified by examining γ-H2AX levels following DNA damage (Figure 5B) and confirmed by examining the average tail moments of cells following cisplatin treatment (Figures 5C, 5D, S5H, and S5I). Next, to explore whether MRE11 lactylation regulated genomic stability, we detected the ratio of chromosome breaks in *MRE11 WT* and *MRE11 K673R* cells and found that cells expressing *MRE11 K673R* showed increased chromosome/chromatid breaks following DNA damage (Figure 5E).

To determine whether lactylation played a key role in DNA damage repair *in vivo*, mice were treated with NALA, CBP inhibitor (CBPi), or LDHi with/without 10 Gy IR. As shown in Figure 5F, increased numbers of γ-H2AX-positive cells were observed in the lung tissue of mice treated with LDHi following IR treatment. Additionally, LDHi treatment significantly decreased phospho-RPA2 levels in lung tissues (Figure S5J). Conversely, NALA treatment markedly decreased the numbers of γ-H2AX-positive cells in lung tissue and increased the intestinal villi length in mice post-IR treatment, but these phenotypes could be reversed by treating mice with CBPi (Figures 5G and 5H). Phospho-RPA2 levels in lung and small intestine tissues were also examined and shown to be consistent with the above results (Figures S5K and S5L). We also constructed *LDHA*-conditional knockout mice to further confirm our findings. As shown in Figures 5I and 5J, knockout of *LDHA* obviously increased the numbers of γ-H2AX-positive cells and decreased the length of intestinal villi in mice post-IR treatment. However, these phenotypes could be rescued by NALA treatment. *LDHA* knockout also obviously decreased IR-induced phospho-RPA2 levels in both lung and intestinal tissues, and these changes were rescued by NALA treatment (Figures 5K, 5L, S5M, and S5N). Taken together, these results suggest that sodium lactylation manipulated by NALA or CBPi regulates DSB repair *in vivo*.

MRE11 lactylation promotes chemoresistance in cancer cells

By analyzing the HRD scores in basal-like breast cancer samples, we found that high *LDHA* expression was associated with lower HRD scores in tumors expressing high levels of *BRCA1* (breast cancer gene 1), implying that high levels of lactate or lactylation could be related to enhanced HR in *BRCA1 WT* cancers (Figure 6A). In addition, given that the high efficacy of DNA damage repair usually leads to chemoresistance,[45] we next examined whether MRE11 lactylation affected chemo-responses in cancer cells. As shown in Figure 6B, NALA treatment led cancer cells to be resistant to olaparib, but CBPi treatment reversed this effect. Furthermore, *MRE11 K673R* cells showed hypersensitivity to olaparib compared with *MRE11 WT* cells (Figures 6C and 6D). Additionally, manipulating lactylation using CBPi or NALA affected chemo-responses in *MRE11 WT* cells but not in *MRE11 K673R* mutant cells (Figures 6C and 6D). These results suggested that MRE11 lactylation regulated chemo-responses in cell-based models.

Previous studies have reported that colon cancer is highly associated with the Warburg effect and generates abundant lactate. This might be a major reason behind chemotherapy resistance in colon cancer.[2,46,47] However, the mechanism underlying these changes remains poorly understood. To examine whether MRE11 lactylation affected colon cancer chemo-responses, we first performed colony formation assays using HCT116 and RKO colon cancer cells. As shown in Figures 6E–6H, LDHi and CBPi treatment both sensitized cancer cells to cisplatin and olaparib. Conversely, NALA treatment led cancer cells to become resistant to cisplatin and olaparib (Figures 6E–6H). Moreover, NALA-mediated chemoresistance was reversed by CBPi treatment (Figures 6G and 6H).

To further confirm the role of MRE11 lactylation in chemoresponse, we performed cancer-killing assays using colon cancer patient-derived organoid (PDO) and patient-derived xenograft (PDX) models. We detected the MRE11 K673 lactylation levels in four different colon cancer PDOs, which were classified into the following two groups: high MRE11 K673 lactylation and low MRE11 K673 lactylation (Figures 6I and S6A–S6D). We found that LDHi and CBPi enhanced cisplatin-killing effects in high lactylation PDOs (220 #, 231 #) (Figures 6J, 6K, and S6E) and that phospho-RPA2 levels were markedly inhibited by LDHi or CBPi treatment in high MRE11 K673 lactylation PDO 220 # after DNA damage (Figure S6F). In PDOs with low MRE11 K673 lactylation (223 #), both NALA and lactic acid treatment promoted resistance to cisplatin (Figures 6L and S6G). Additionally, phospho-RPA2 levels were significantly increased by NALA or lactic acid treatment in low MRE11 K673 lactylation PDOs (Figure S6H).

Next, we screened three colon cancer PDXs by examining their MRE11 K673 lactylation levels and then selected the highest lactylated PDX to perform cancer-killing assays *in vivo* (Figure 6M). As shown in Figures 6N–6P, both CBPi and LDHi significantly enhanced the killing effects of olaparib on the high K673 lactylation colon PDX. In addition, CBPi and LDHi also markedly decreased phospho-RPA2, Ki67, and MRE11-K673la staining but increased γ-H2AX staining in olaparib treatment groups, suggesting that CBPi and LDHi inhibited DNA end resection and impaired DNA damage repair *in vivo*, which in turn led to cancer sensitivity to chemotherapy (Figures S6I–S6M). Taken together, these results suggest

that combining CBPi or LDHi with chemotherapy might be a potentially effective strategy to treat cancer with high levels of MRE11 K673 lactylation.

Inhibiting MRE11 K673 lactylation with a peptidic inhibitor enhances chemotherapy sensitivity

Since targeting *CBP* or *LDH* affects multiple signaling pathways, a strategy that specifically targets MRE11 K673 lactylation is also needed. Based on motifs involved in protein PTMs, specifically generated peptides have been shown to be a promising and effective strategy to inhibit protein's PTMs.[48,49] After analyzing the sequence around the MRE11 K673 site, we synthesized five short peptides fused with CPPs,[50–52] which have become one of the most popular and effective tools for the intracellular delivery of biomolecules (Figure 7A). K673-peptide-3# (termed as K673-pe) presented the strongest inhibitory effect on MRE11 lactylation (Figure 7B). Thus, based on the K673-pe peptide, we synthesized a scrambled peptide (termed as K673R-pe), where the K673 residue was substituted with an R residue. As shown in Figures 7C, 7D, and S7A–S7C, K673-pe, but not K673R-pe, markedly decreased MRE11 lactylation, which in turn decreased cisplatin-induced phospho-RPA2 levels (Figure 7E). Moreover, K673-pe significantly inhibited MRE11-K673la and RPA2 foci formation in response to DNA damage (Figures 7F–7H), implying that K673-pe inhibits MRE11 K673 lactylation and results in significant decreases in DNA end resection. Furthermore, K673-pe treatment also decreased RAD51 foci, which is consistent with a sharp reduction in HR levels in K673-pe treated cells (Figures 7F, 7I, and 7J). These results suggested that peptide K673-pe could downregulate HR by inhibiting MRE11 lactylation.

We next asked whether K673-pe treatment could sensitize cancer cells to chemotherapy. As shown in Figures 7K, 7L, S7D, and S7E, K673-pe, but not K673R-pe, significantly enhanced cancer cell sensitivity to olaparib and cisplatin. Additionally, K673-pe led *MRE11 WT* cells, but not *MRE11 K673R* cells, to become further sensitive to cisplatin (Figure 7M), suggesting that K673-pe regulates chemo-responses by inhibiting MRE11 lactylation.

To further confirm the synergistic killing effect of combination K673-pe and chemotherapy *in vivo*, the highest MRE11K673 lactylation colon cancer PDX model was used for further cancer-killing assays. The peptide K673-pe did not have obvious toxic effects in mice, as indicated by the survival rate and normal renal/liver function (Figures S7F–S7P). As shown in Figures 7N and 7O, K673-pe, but not K673R-pe, significantly sensitized colon PDX to olaparib. Additionally, K673-pe sharply decreased phospho-RPA2, Ki67, and MRE11-K673la but increased γ-H2AX staining in olaparib treatment groups (Figures S7Q–S7U). Taken together, these results suggest that targeting MRE11 K673 lactylation with K673-pe may enhance chemotherapy effects in cancer with high MRE11 K673 lactylation levels.

DISCUSSION

The Warburg effect is a common phenomenon in most cancers and is associated with the production of large amounts of lactate.[53] Despite being discovered over 90 years ago, the role of the Warburg byproduct lactate plays in cancer cells remains largely unknown.[53] Recently, it has been reported that lactate is a major source of histone protein lactylation-a recently defined PTM.[6] Previous studies have shown that lactate promotes

chemoresistance.[2,47,54,55] However, the precise mechanism of this phenotype remains to be explored.

HR, one of the most important DNA damage repair pathways, is error-free and plays a key role in maintaining genomic stability and inhibiting tumorigenesis.[56] However, overactivation of HR in cancer has been implicated in chemoresistance.[57] MRE11, the core component of the MRN complex, is responsible for DNA binding and cutting.[23,25,38,58] After DSBs occur, MRE11 is recruited to damage sites to initiate DNA end resection.[59] Next, the exonuclease EXO1/DNA2 is recruited to the DNA damage sites and mediates the extensive resection, which is pivotal for the HR repair process.[60,61] Thus, the recruitment of MRE11 to DNA is a vital step for the MRE11-mediated initiation of DNA resection and HR repair.

Dysregulation of MRE11 results in immunodeficiency, radiation sensitivity, defective cell-cycle checkpoints, and an increased predisposition to the development of cancer.[59,62] Thus, the precise regulation of MRE11 is vital for safeguarding genome stability and cell viability.[63] PTMs of MRE11 play an important role in regulating its functions. Ubiquilin 4 (UBQLN4, a key member of the ubiquitin-like protein family)-mediated ubiquitination of MRE11 leads to its degradation and thus affects DSB repair pathway choice.[44] UFMylation of MRE11 on K282 by UFL1 (UFM1 specific ligase 1) is essential for optimal ATM activation, HR-mediated DSB repair, and genome integrity.[64] PLK1-mediated MRE11 phosphorylation decreases its ability to bind to DNA, resulting in the inhibition of HR repair.[65] Arginine methylation of MRE11 by protein arginine methyltransferase 1 (PRMT1, a conserved enzyme in the evolution of the arginine methyltransferase family) at its GAR domain regulates its exonuclease activity.[66] Additionally, C1QBP promotes MRE11 stability but inhibits its exonuclease activity by impeding its DNA binding through interactions with MRE11.[67] dynein light chain LC8-type 1 (DYNLL1) and Nej1, the yeast homolog of XLF (non-homologous end joining factor 1), have also been reported to directly bind with MRE11 and then inhibit MRE11 resection activity.[68,69] Current models suggest that MRE11 binds to DNA in RAD50-dependent and -independent manners.[23,35–39] However, the regulation and mechanism underlying MRE11 recruitment to DNA after DNA damage remain largely unknown.

In this study, we found that MRE11 was lactylated by CBP. After DNA damage, interactions between MRE11 and CBP were increased, and MRE11 lactylation was increased. MRE11 was specifically lactylated at its second DBD, K673. Interestingly, our findings suggested that MRE11 K673 lactylation enhanced its DNA-binding ability and then promoted end resection and HR repair. High MRE11 K673 lactylation resulted in high efficacy of HR repair and chemoresistance. However, the combination of a CBPi or LDHi (which inhibits MRE11 lactylation) and chemotherapy significantly attenuated HR repair and increased cancer-killing effects. We also performed cancer-killing assays using a high lactylation colon cancer PDX model *in vivo* and found that inhibition of MRE11 K673 lactylation significantly enhanced PARPi-mediated cancer-killing effects. We also designed and generated CPPs that could specifically inhibit MRE11 K673 lactylation. These peptides could inhibit DNA end resection and impair DNA damage repair. Additionally, a

combination of the peptide and chemotherapy (cisplatin or olaparib) significantly promoted chemotherapy-mediated cancer cell-killing effects *in vitro* and *in vivo*.

Collectively, our findings implicate a player in HR repair: MRE11 lactylation. MRE11 lactylation also connects cancer metabolism with DSB repair. Considering that the Warburg effect is a common phenomenon in most cancers that produce large amounts of lactate, protein lactylation may enhance HR repair in cancer and lead to chemoresistance. DNA damage also enhances MRE11 lactylation by activating CBP. Thus, the internal driver (the Warburg effect-induced lactate formation) and external driver (chemotherapy-induced hyperlactylation-MRE11) may synergistically drive the overactivation of HR in cancer development and therapeutic processes, leading to chemoresistance. Our findings imply that lactylation may serve as a biomarker for PARPi treatment to supplement BRCA status. Additionally, for cancers with high MRE11 K673 lactylation levels, combining a CBPi, LDHi, or K673-pe with platinum or PARPi may help overcome chemoresistance.

Limitations of the study

Although we found that MRE11 lactylated at K673 by CBP is important for DNA end resection and MRE11 is acetylated at K609 by GCN5, the functional significance of MRE11 acetylation remains to be further studied. Second, although our findings determined that MRE11 lactylation promotes its binding to DNA, the precise mechanism and structure information of MRE11 lactylation remain to be further explored. Unlike acetylation of lysine (K), which could be mimicked by K to Q (glutamine) mutation, there is no effective mutation of lysine (K) to mimic lactylation to date. Hence, we cannot genetically generate MRE11 K673 lactylation mimicking mice to study the roles of MRE11 K673 lactylation in HR repair *in vivo*.

STAR★METHODS

RESOURCE AVAILABILITY

Lead contact—Further information and requests for resources and reagents should be directed to and will be fulfilled by the lead contact, Jian Yuan (yuanjian229@hotmail.com).

Materials availability—All primary cells, plasmids, and mouse strains generated in this study are available from the lead contact with a completed materials transfer agreement.

Data and code availability

- The original western-blot images, mass spectrometry data, and microscopy data reported in this paper will be shared by the lead contact upon request.
- No original code was used in this study.
- Any additional information required to reanalyze the data reported in this paper is available from the lead contact upon request.

EXPERIMENTAL MODEL AND STUDY PARTICIPANT DETAILS

The sequences of qPCR assay primer, the target sequences for Knockdown of *MRE11*, *CBP*, *GCN5*, and the sequences of 70bp-dsDNA and 55bp-Overhang DNA for electrophoretic mobility shift assay (EMSA) are provided (Table S1).

Animal—All animal experiments and procedures were carried out in strict accordance with the Guidelines for the Care and Use of Laboratory Animals set by the U.S. National Institutes of Health (National Academies Press; 2011) and and were performed following the ethical guidelines protocols approved by Tongji University school of medicine.

Generation of *LDHA* Knockout Mice model—$LDHA^{fl/fl}$ mice were generated based on the C57BL/6N strain using CRISPR/Cas9 by Shanghai Model Organisms. Subsequently, $LDHA^{fl/fl}$ mice and UBC-Cre^{ERT} were utilized to generate UBC-Cre +/− $LDHA^{fl/fl}$ mice. To achieve Cre mediated recombination, mice were treated with tamoxifen (T5648, Sigma) dissolved in corn oil via intraperitoneal injection (80 mg/kg, once a day for 7 consecutive days).

Sodium Lactate treatment *in vivo*—For *in vivo* animal experiments, sodium lactate (120 mg.kg-1) was intraperitoneally injected mice once a day.

Intestinal villi regeneration assay—For normal C57BL6 mice, 8–12-week-old mice (5 mice per group) were intraperitoneally pre-treated with LDHi (Sodium oxamate) (1000 mg.kg-1, once/two days), CBPi (15 mg.kg-1, once/two days) or sodium lactate (120 mg.kg-1, once a day) alone or combined as indicate 5 day before 10 Gy whole-body irradiation and housed in a specific pathogen-free environment. After irradiation, mice were continuously treated as mentioned above for another 5 days before being sacrificed. The small intestines were used for histological analyses.

For *LDHA* knockout mice, 8–12-week-old mice (5 mice per group) were pre-treated with/without sodium lactate (120 mg.kg-1, once a day) for 5 days before 6 Gy whole-body irradiation and housed in a specific pathogen-free environment. After irradiation, mice were treated with/without sodium lactate for another 5 days before sacrificed. The small intestines were used for histological analyses.

Patient-derived xenograft models—Colon cancer patient-derived xenografts (PDXs) were subcutaneously transplanted into 6-week-old female nu/nu mice. Mice bearing tumors of 150–200 mm^3 were randomly assigned into six groups: vehicle control group (saline), sodium oxamate group (1000 mg.kg-1), CBPi group (15 mg.kg-1), olaparib group (50 mg.kg-1), olaparib (50 mg.kg-1)+sodium oxamate (1000 mg.kg-1) group and Olaparib (50 mg.kg-1)+ CBPi (15 mg.kg-1) group. The treated mice were intraperitoneally injected three times/week. Tumor volume was measured and measured as mentioned in tumor xenograft assay.

For assays testing the combination of K673-pe or K673R-pe and olaparib to kill colon cancer PDXs, mice bearing tumors of 150–200 mm^3 as mentioned above were also randomly assigned into six groups: vehicle control group (saline), K673R-pe (5 mg.kg-1)

group, K673-pe (5 mg.kg-1) group, olaparib group (50 mg.kg-1), olaparib (50 mg.kg-1) + K673R-pe (5 mg.kg-1) group and olaparib (50 mg.kg-1) + K673-pe (5 mg.kg-1) group. K673-pe or K673R-pe were intraperitoneally injected once a day and olaparib were intraperitoneally injected three times/week.

Patient-derived organoid models—Four colon cancer organoids were first used to measure MRE11 K673 lactylation levels by western blot. Furthermore, these organoids were divided into two groups, high MRE11 K673 lactylation and low MRE11 K673 lactylation, according to their MRE11 K673 lactylation levels. Organoids in good condition were passaged and seeded in standard 96-well cell culture plates (Corning). The organoids with high MRE11 K673 lactylation levels were treated by cisplatin (65μM) alone or in combination with LDHi (30mM, 40mM) or CBPi (50μM, 60μM) as indicated. The organoids with low MRE11 K673 lactylation levels were treated with cisplatin (65μM) alone or in combination with L-lactate (15mM, 20mM) or sodium lactate (60mM, 80mM) as indicated. After 72h, the organoids growth was examined by CCK8.

Cell culture and treatment—HEK293T, U2OS, the breast cancer cell line MDA-MB-231 and the colon cancer cell lines HCT116 and RKO were purchased from ATCC. Unless otherwise stated, cells were cultured in DMEM supplemented with 10% fetal bovine serum (FBS) at 37°C in 5% (v/v) CO_2. For western blot assays, cells were usually treated with cisplatin at a concentration of 20 μM, bleomycin at a concentration of 20 μM, CBPi at a concentration of 10 μM, MCT1/4i at a concentration of 10 μM or 20 μM, target Mre11K673 lactylation peptides at a concentration of 20 μM, LDHi (sodium oxamate) at a concentration of 10 mM or 20 mM, NALA (Sodium lactate) at a concentration of 10 mM, 25 mM or 50 mM, NAAC (Sodium acetate) at a concentration of 25 mM or 50 mM, L-lactate at a concentration of 10 mM or 20 mM for 24 h. For immunofluorescence assays, cells were usually treated with cisplatin at a concentration of 10 μM, bleomycin at a concentration of 10 μM, CBPi at a concentration of 10 μM, targeted Mre11K673 lactylation peptides at a concentration of 20 μM, LDHi at a concentration of 10 mM, NALA at a concentration of 25 mM. For qPCR assays, cells were usually treated with NALA at a concentration of 20 mM, L-lactate at a concentration of 20 mM for 24 h. For colony formation assays, cells were usually treated with CBPi at a concentration of 5 μM, LDHi at a concentration of 10 mM, NALA at a concentration of 10 mM or 25 mM, L-lactate at a concentration of 10 mM. For CCK-8 assays, cells were usually treated with targeted Mre11 K673 lactylation peptides at a concentration of 20 μM.

METHOD DETAILS

DNA transfection, virus packaging and lentiviral infection—Cells were transfected with Polyetherimide (PEI) or Lipofectamine 2000/3000 (Thermo Fisher Scientific). Viral supernatant was collected two times (24 h and 48 h) after the co-transfection of lentiviral vectors and packaging plasmids (pMD2G and psPAX2). Harvested lentiviruses were added to the cells for further experiments with 8 μg/ml polybrene which enhances infection efficiency. Stable cells were selected with media containing 2 μg/mL puromycin. The stable cells were detected by immunoblotting.

HR report assay—DR-GFP reporter systems were employed to examine DSB repair efficiency. Briefly, HEK293T cells stably expressing the indicated shRNA or normal HEK293T cells were seeded into six-well plates in triplicate. 24 h later, cells in each well were transfected with a complex that contained 3μl Polyetherimide (PEI), 500 ng *DR-GFP*, 100 ng *mCherry*, and 500 ng *I-SceI* plasmids which were employed to generated DNA double strands breaks(DSBs). After transfection 24 h, cells were treated with indicated reagents. After transfection 48 h, cells were harvested and analyzed by flow cytometric analysis (FACS), sorting by RFP-positive cells or RFP/GFP both positive cells. The ratio of repair efficiency was calculated as described previously.[42]

Immunofluorescence—Cells were seeded into six-well plates with coverslips 24 h before treatment. For RRA2 foci staining, cells were fixed with methanol: acetone (1:1) at −20°C for 20 min. Cells were washed two times using PBS and fixed again with 4% PFA at room temperature for 15 min. For RAD51 staining, cells were pre-extracted 10 min on ice with pre-extraction buffer (20 mM HEPES, pH 7.4, 20 mM NaCl, 5 mM $MgCl_2$, 0.5% NP-40, 1 mM DTT and protease inhibitor cocktails) followed by 10 min 4% PFA fixation. Before staining, cells were blocked with 2% goat serum for 1 h at RT. Next, cells were incubated with primary antibodies overnight at 4°C. After washing 3 times with PBS, cells were incubated with secondary antibodies at room temperature for 1 h. After washing 3 times with PBS, cells were incubated with DAPI at room temperature for about 2 min. After washing, cells were mounted with anti-fade solution and visualized using Fluorescence microscope.

End resection detection with BrdU staining—U2OS cells seeded on cover slides were pre-incubated with 10 μg/ml BrdU for 16 h and then were treated with cisplatin for 12 h. cells were washed with PBS and then released with buffer 1 (10 mM PIPES, pH 7.0, 100 mM NaCl, 300 mM Sucrose, 3 mM $MgCl_2$, 0.5% Triton X-100) on ice for 10 min. Next, cells were washed using PBS and re-released with buffer 2 (10 mM Tris-HCl, pH 7.5; 10 mM NaCl; 3 mM $MgCl_2$, 1% Tween-40, 0.5% sodium deoxycholate) on ice for another 10 min. After wash, cells were fixed with 4% PFA at room temperature for 30 min. The slides were blocked 5% BSA and then incubated with anti-BrdU (1:100) primary antibody at 4°C overnight. Secondary antibody and DAPI staining were performed as mentioned above.

Detection of end resection using qPCR—Stably expressing *MRE11 WT* or *K673R* mutant AsiSI-ER U2OS cells[70] which endogenous MRE11 were depleted were treated with 300 nM 4-OHT for 4 h or mock-treated. Genomic DNA was extracted. The genomic DNA sample (~500 ng) was digested or mock-digested with the restriction enzyme BamH1 (New England Biolabs) at 37°C overnight. The digested or mock-digested samples (~50 ng) were used as templates in 20 μl of qPCR reaction containing 10 μl of 2 * Taqman Universal PCR Master Mix (Applied Biosystems), 0.5 μM of each primer and 0.2 μM probe using the StepOne Plus Real-Time PCR System (Applied Biosystems). The primer sequences were described in previous publications.[71] The percentage of single-stranded DNA (ssDNA%) generated by resection at selected sites was calculated as: $ssDNA\% = 1/(2^{(\Delta Ct - 1)} + 0.5) *100$.

Mass spectrometry analysis—To identify MRE11 lactylation sites, 293T cells stably expressing HA-tagged MRE11 were treated with 50 mM NALA for 24 h before harvest and then lysed. The lysates were purified using anti-HA-agarose beads. The pellet was then resolved on SDS–PAGE and stained with Coomassie blue staining. The band corresponding to HA-MRE11 was excised and sent for mass spectrometry analysis.

Measurement of Lactate levels—Intracellular lactate level was measured by using lactate Colorimetric/Fluorometric assay kit (Abcam ab65331) according to manufacturer's protocol.

Co-immunoprecipitation and Western blotting—For transient transfection and co-immunoprecipitation assays, constructs encoding *HA-tagged MRE11* or *HA-tagged CBP* constructs were transiently co-transfected into HEK293T cells. The transfected cells were lysed with NETN buffer (20 mM Tris–HCl, pH 8.0, 100 mM NaCl, 1 mM EDTA, and 0.5% Nonidet P-40) containing 1 × protease inhibitors on ice for 25 min. After removal of cell debris by centrifugation at 12000rpm for 10 minutes, the soluble fractions were collected and incubated with HA beads for 2h at 4°C. Beads were washed three times with NETN buffer, boiled in 1 × SDS loading buffer for 5 min, and resolved on SDS–PAGE. Membranes were blocked using 5% milk in TBST buffer and then probed with antibodies as indicated.

Metaphase spreads—For metaphase spreads, MDA-MB-231 cells were treated with or without olaparib (1 μM) overnight and arrested with colcemid (0.1 μg/mL) at 37 C° for 6–8 h and then harvested, resuspended in prewarmed hypotonic solution (75 mM KCl) at 37 C° for about 20 min. After the samples were centrifuged (1000 RPM, 5 min) and supernatant discarded, cells were fixed twice using carnoy's buffer (methanol-acetic acid (3:1 (v/v)) at RT for 10 min each time. The cells were centrifuged (1000 RPM, 5 min) and then the supernatant was discarded. Next, the cells were re-suspended with carnoy's buffer and then dropped onto slides, dried for about 30 min at RT. Slides were stained using 5% Giemsa (Sigma) for 5 min. Genomic instability was analyzed by counting cells which showed chromosome breaks or loss.

HRD score analysis—TCGA breast cancer cohort HRD scores were published earlier and downloaded from the Genomic Data Commons (GDC).[72,73] Expression data as log transformed TPM was downloaded from UCSC xenabrowser.[74] HRD scores analysis was performed on basal subtype (n=140) as defined by PAM50 signature as previously defined. Samples were subgrouped by median expression levels of *BRCA1* and *LDHA*. Statistical significance was tested by two-sided Mann-whitney-Wilcoxon test.

Expression and purification of recombinant proteins—Bacterial expression constructs (pGEX-4T-2) containing the indicated genes were transformed into Escherichia coli BL-21. Cells were induced to express protein using 0.5mM IPTG (isopropyl-β-D-thiogalactopyranoside) at 18 °C with 180 RPM rotation overnight. Cells were re-suspended in PBS containing 0.5% Triton X-100 and 2 mM β-mercaptoethanol, followed by ultrasonication. The proteins were purified using glutathione beads according to the manufacturer's protocol (Amersham Bioscience).

Soluble Fractions Extraction and Chromatin Fractions Extraction—First, cells were lysed with NETN buffer (20 mM Tris–HCl, pH 8.0, 100 mM NaCl, 1 mM EDTA, and 0.5% Nonidet P-40) containing 1× protease inhibitors on ice for 10 min. After the centrifugation (12,000 RPM for 10 min at 4°C), the supernatant was collected as the whole cell extract. The remaining pellet were washed at least 3 times using PBS buffer and further lysed with cold EBC2 buffer (50 mM Tris-HCl, pH 7.5, 300 mM NaCl, 5mM $CaCl_2$, and 10 U microcal nuclease). After sonication and centrifugation (12,000 RPM for 10 min at 4 °C), the supernatants were collected as chromatin fractions.

Colony formation assay—The indicated cells (500–2000) were seeded in triplicate in each well of six-well plates. For chemotherapy sensitivity assay, after 1 day, cells were exposed to indicated drug at the indicated doses, and left for 10–14 days in the incubator to allow colony formation. Colonies were stained with GIEMSA and quantified. Results were normalized to plating efficiencies.

Electrophoretic Mobility Shift Assay—The indicated concentrations of MRE11 proteins were incubated with dsDNA or overhang DNA substrate in reaction buffer (25 mM Tris-HCl, pH 7.5, 5 mM $MgCl_2$, 1 mM DTT, 100 mg/ml BSA, 2 mM ATP) containing 100 mM KCl at 37°C for 15 min. After incubation, the reactions were mixed with loading buffer (20 mM Tris-HCl, pH 7.5, 40% glycerol, 2 mM EDTA, 0.2% orange G) and then separated by electrophoresis using a 0.5% agarose gel in SB buffer (10 mM NaOH, 40 mM boric acid, pH 8.0), as previously published.[67]

Comet assay—Stably expressing *MRE11 WT* or *MRE11 K673R* MDA-MB-231 cells with endogenous MRE11 depleted were seeded into 6-well plates with a density of 1 × 10^5 cells per well. After treatment with cisplatin as indicated, cells were harvested at the indicated time and then utilized for Comet assays according to the manufacturer's instructions. Briefly, cells were embedded in low melting agarose on a glass slide and then immersed in lysis buffer for 1 h at 4 °C. Slides were then incubated with 1 × electrophoresis buffer for about 40 min to unwind DNA. Subsequently, electrophoresis was performed for 25 min at 25 V. Next, the slide was stained with PI and then covered by cover-glass. For quantification, comets on each gel were observed using a fluorescence microscope. Tail length and tail moment were measured to evaluate the degree of DNA damage.

***In vitro* lactylation assay—**The GST fusion MRE11 proteins were incubated with HA-tagged CBP proteins which were purified from HEK293T cells in reaction buffer (50 mM HEPES, pH7.8, 30 mM KCl, 0.25 mM EDTA, 5.0 mM $MgCl_2$, 5.0 mM sodium butyrate, 2.5 mM DTT) with 20 μM lactyl-CoA. Reactions were incubated at 30°C for 30 min. Next, 5 × SDS loading buffer was added to the reaction and boiled for 5 min at 100°C. Samples were separated by SDS-PAGE and immunoblotted with indicated antibodies.

Peptide synthesis—All peptides were synthetized by Guoping Pharmaceutic Inc (Hefei, China). Synthetic peptides were purified to >98% purity by high-pressure liquid chromatography for both *in vitro* and *in vivo* use. The amino acids of peptides used *in vivo* use were all D isoforms. For *in vitro* experiments, peptides were dissolved in PBS to generate a 10 mM stock solution. For *in vivo* use, K673-pe and K673R-pe were dissolved

in PBS and kept on ice until injection. Before injection, the solution was brought to room temperature.

QUANTIFICATION AND STATISTICAL ANALYSIS

For cell survival, PDOs, PDXs xenograft and RPA2, MRE11, RDA51, BrdU and MRE11-K673la foci assay, data are represented as the mean ± S.E.M of three independent experiments. For the animal study, data are represented as the mean ± S.E.M of 5 mice. Statistical analyses were performed in GraphPad Prism with the Student's t-test.

Supplementary Material

Refer to Web version on PubMed Central for supplementary material.

ACKNOWLEDGMENTS

We thank Dr. Xingzhi Xu for providing purified RAD50 protein and Dr. Gaëlle Legube for the AsiSI-ER U2OS cell line. This work was supported by the National Natural Science Foundation of China (82225035 to J. Yuan), the National Key R&D Program of China (2022YFA1302803 to J. Yuan), the National Natural Science Foundation of China (32090032 to J. Yuan, 82002985 to Y.C., 82172994 to Y.C., and 32070713 to J. Yuan), the Shanghai Pujiang program (2020PJD070 to Y.C.), the China Postdoctoral Science Foundation (2021T140516 to Y.C., 2020M681384 to Y.C., and BX20220232 to J. Wu), the Natural Science Foundation of Shanghai Municipality (22XD1422300 to J. Yuan), the Shanghai Municipal Health Commission (2022XD053 to J. Yuan), and the Shanghai Municipal Human Resources and Social Security Bureau (2022754 to J. Wu).

REFERENCES

1. Vander Heiden MG, Cantley LC, and Thompson CB (2009). Understanding the Warburg effect: the metabolic requirements of cell proliferation. Science 324, 1029–1033. [PubMed: 19460998]
2. de la Cruz-López KG, Castro-Muñ oz LJ, Reyes-Hernández DO, García-Carrancá A, and Manzo-Merino J (2019). Lactate in the regulation of tumor microenvironment and therapeutic approaches. Front. Oncol 9, 1143. [PubMed: 31737570]
3. Hsu PP, and Sabatini DM (2008). Cancer cell metabolism: Warburg and beyond. Cell 134, 703–707. [PubMed: 18775299]
4. Liu KX, Everdell E, Pal S, Haas-Kogan DA, and Milligan MG (2021). Harnessing lactate metabolism for radiosensitization. Front. Oncol 11, 672339.
5. Xie H, Hanai J, Ren JG, Kats L, Burgess K, Bhargava P, Signoretti S, Billiard J, Duffy KJ, Grant A, et al. (2014). Targeting lactate dehydrogenase–a inhibits tumorigenesis and tumor progression in mouse models of lung cancer and impacts tumor-initiating cells. Cell Metab. 19, 795–809. [PubMed: 24726384]
6. Zhang D, Tang Z, Huang H, Zhou G, Cui C, Weng Y, Liu W, Kim S, Lee S, Perez-Neut M, et al. (2019). Metabolic regulation of gene expression by histone lactylation. Nature 574, 575–580. [PubMed: 31645732]
7. Papamichos-Chronakis M, and Peterson CL (2013). Chromatin and the genome integrity network. Nat. Rev. Genet 14, 62–75. [PubMed: 23247436]
8. Draviam VM, Xie S, and Sorger PK (2004). Chromosome segregation and genomic stability. Curr. Opin. Genet. Dev 14, 120–125. [PubMed: 15196457]
9. Quinet A, Tirman S, Cybulla E, Meroni A, and Vindigni A (2021). To skip or not to skip: choosing repriming to tolerate DNA damage. Mol. Cell 81, 649–658. [PubMed: 33515486]
10. Schwertman P, Bekker-Jensen S, and Mailand N (2016). Regulation of DNA double-strand break repair by ubiquitin and ubiquitin-like modifiers. Nat. Rev. Mol. Cell Biol 17, 379–394. [PubMed: 27211488]

11. Di Virgilio M, Callen E, Yamane A, Zhang W, Jankovic M, Gitlin AD, Feldhahn N, Resch W, Oliveira TY, Chait BT, et al. (2013). Rif1 prevents resection of DNA breaks and promotes immunoglobulin class switching. Science 339, 711–715. [PubMed: 23306439]
12. Arnould C, Rocher V, Finoux AL, Clouaire T, Li K, Zhou F, Caron P, Mangeot PE, Ricci EP, Mourad R, et al. (2021). Loop extrusion as a mechanism for formation of DNA damage repair foci. Nature 590, 660–665. [PubMed: 33597753]
13. Ramsden DA, Carvajal-Garcia J, and Gupta GP (2022). Mechanism, cellular functions and cancer roles of polymerase-theta-mediated DNA end joining. Nat. Rev. Mol. Cell Biol 23, 125–140. [PubMed: 34522048]
14. Xu G, Chapman JR, Brandsma I, Yuan J, Mistrik M, Bouwman P, Bartkova J, Gogola E, Warmerdam D, Barazas M, et al. (2015). REV7 counteracts DNA double-strand break resection and affects PARP inhibition. Nature 521, 541–544. [PubMed: 25799992]
15. Callen E, Di Virgilio M, Kruhlak MJ, Nieto-Soler M, Wong N, Chen HT, Faryabi RB, Polato F, Santos M, Starnes LM, et al. (2013). 53BP1 mediates productive and mutagenic DNA repair through distinct phosphoprotein interactions. Cell 153, 1266–1280. [PubMed: 23727112]
16. Weinstock DM, Richardson CA, Elliott B, and Jasin M (2006). Modeling oncogenic translocations: distinct roles for double-strand break repair pathways in translocation formation in mammalian cells. DNA Repair (Amst) 5, 1065–1074. [PubMed: 16815104]
17. Orthwein A, Noordermeer SM, Wilson MD, Landry S, Enchev RI, Sherker A, Munro M, Pinder J, Salsman J, Dellaire G, et al. (2015). A mechanism for the suppression of homologous recombination in G1 cells. Nature 528, 422–426. [PubMed: 26649820]
18. Zhao F, Kim W, Kloeber JA, and Lou Z (2020). DNA end resection and its role in DNA replication and DSB repair choice in mammalian cells. Exp. Mol. Med 52, 1705–1714. [PubMed: 33122806]
19. Anand R, Ranjha L, Cannavo E, and Cejka P (2016). Phosphorylated CtIP functions as a co-factor of the MRE11-RAD50-NBS1 endonuclease in DNA end resection. Mol. Cell 64, 940–950. [PubMed: 27889449]
20. Paull TT (2021). Reconsidering pathway choice: a sequential model of mammalian DNA double-strand break pathway decisions. Curr. Opin. Genet. Dev 71, 55–62. [PubMed: 34293662]
21. Limbo O, Chahwan C, Yamada Y, de Bruin RA, Wittenberg C, and Russell P (2007). Ctp1 is a cell-cycle-regulated protein that functions with Mre11 complex to control double-strand break repair by homologous recombination. Mol. Cell 28, 134–146. [PubMed: 17936710]
22. Kanaar R, and Wyman C (2008). DNA repair by the MRN complex: break it to make it. Cell 135, 14–16. [PubMed: 18854148]
23. Williams RS, Moncalian G, Williams JS, Yamada Y, Limbo O, Shin DS, Groocock LM, Cahill D, Hitomi C, Guenther G, et al. (2008). Mre11 dimers coordinate DNA end bridging and nuclease processing in double-strand-break repair. Cell 135, 97–109. [PubMed: 18854158]
24. van den Bosch M, Bree RT, and Lowndes NF (2003). The MRN complex: coordinating and mediating the response to broken chromosomes. EMBO Rep. 4, 844–849. [PubMed: 12949583]
25. Buis J, Wu Y, Deng Y, Leddon J, Westfield G, Eckersdorff M, Sekiguchi JM, Chang S, and Ferguson DO (2008). Mre11 nuclease activity has essential roles in DNA repair and genomic stability distinct from ATM activation. Cell 135, 85–96. [PubMed: 18854157]
26. Escribano-Díaz C, Orthwein A, Fradet-Turcotte A, Xing M, Young JT, Tkáč J, Cook MA, Rosebrock AP, Munro M, Canny MD, et al. (2013). A cell cycle-dependent regulatory circuit composed of 53BP1-RIF1 and BRCA1-CtIP controls DNA repair pathway choice. Mol. Cell 49, 872–883. [PubMed: 23333306]
27. Scully R, Panday A, Elango R, and Willis NA (2019). DNA double-strand break repair-pathway choice in somatic mammalian cells. Nat. Rev. Mol. Cell Biol. 20, 698–714. [PubMed: 31263220]
28. Chen G, Chen J, Qiao Y, Shi Y, Liu W, Zeng Q, Xie H, Shi X, Sun Y, Liu X, et al. (2018). ZNF830 mediates cancer chemoresistance through promoting homologous-recombination repair. Nucleic Acids Res. 46, 1266–1279. [PubMed: 29244158]
29. Ray Chaudhuri A, Callen E, Ding X, Gogola E, Duarte AA, Lee JE, Wong N, Lafarga V, Calvo JA, Panzarino NJ, et al. (2016). Replication fork stability confers chemoresistance in BRCA-deficient cells. Nature 535, 382–387. [PubMed: 27443740]

30. Russo M, Crisafulli G, Sogari A, Reilly NM, Arena S, Lamba S, Bartolini A, Amodio V, Magrì A, Novara L, et al. (2019). Adaptive mutability of colorectal cancers in response to targeted therapies. Science 366, 1473–1480. [PubMed: 31699882]

31. Wu W, and Zhao S (2013). Metabolic changes in cancer: beyond the Warburg effect. Acta Biochim. Biophys. Sin. (Shanghai) 45, 18–26. [PubMed: 23257292]

32. Valvona CJ, Fillmore HL, Nunn PB, and Pilkington GJ (2016). The regulation and function of lactate dehydrogenase A: therapeutic potential in brain tumor. Brain Pathol. 26, 3–17. [PubMed: 26269128]

33. Wagner W, Ciszewski WM, and Kania KD (2015). L- and D-lactate enhance DNA repair and modulate the resistance of cervical carcinoma cells to anticancer drugs via histone deacetylase inhibition and hydroxycarboxylic acid receptor 1 activation. Cell Commun. Signal. 13, 36. [PubMed: 26208712]

34. Gaffney DO, Jennings EQ, Anderson CC, Marentette JO, Shi T, Schou Oxvig AM, Streeter MD, Johannsen M, Spiegel DA, Chapman E, et al. (2020). Non-enzymatic lysine Lactoylation of glycolytic enzymes. Cell Chem. Biol. 27, 206–213.e6. [PubMed: 31767537]

35. de Jager M, Dronkert ML, Modesti M, Beerens CE, Kanaar R, and van Gent DC (2001). DNA-binding and strand-annealing activities of human Mre11: implications for its roles in DNA double-strand break repair pathways. Nucleic Acids Res. 29, 1317–1325. [PubMed: 11238998]

36. Sun J, Lee KJ, Davis AJ, and Chen DJ (2012). Human Ku70/80 protein blocks exonuclease 1-mediated DNA resection in the presence of human Mre11 or Mre11/Rad50 protein complex. J. Biol. Chem. 287, 4936–4945. [PubMed: 22179609]

37. Déry U, Coulombe Y, Rodrigue A, Stasiak A, Richard S, and Masson JY (2008). A glycine-arginine domain in control of the human MRE11 DNA repair protein. Mol. Cell. Biol. 28, 3058–3069. [PubMed: 18285453]

38. Paull TT (2018). 20 years of Mre11 biology: no end in sight. Mol. Cell 71, 419–427. [PubMed: 30057197]

39. Park YB, Chae J, Kim YC, and Cho Y (2011). Crystal structure of human Mre11: understanding tumorigenic mutations. Structure 19, 1591–1602. [PubMed: 22078559]

40. Di Virgilio M, Ying CY, and Gautier J (2009). PIKK-dependent phosphorylation of Mre11 induces MRN complex inactivation by disassembly from chromatin. DNA Repair (Amst) 8, 1311–1320. [PubMed: 19709933]

41. Kijas AW, Lim YC, Bolderson E, Cerosaletti K, Gatei M, Jakob B, Tobias F, Taucher-Scholz G, Gueven N, Oakley G, et al. (2015). ATM-dependent phosphorylation of MRE11 controls extent of resection during homology directed repair by signalling through exonuclease 1. Nucleic Acids Res. 43, 8352–8367. [PubMed: 26240375]

42. Zhao F, Kim W, Gao H, Liu C, Zhang Y, Chen Y, Deng M, Zhou Q, Huang J, Hu Q, et al. (2021). ASTE1 promotes shieldin-complex-mediated DNA repair by attenuating end resection. Nat. Cell Biol. 23, 894–904. [PubMed: 34354233]

43. Wagner SA, Beli P, Weinert BT, Nielsen ML, Cox J, Mann M, and Choudhary C (2011). A proteome-wide, quantitative survey of in vivo ubiquitylation sites reveals widespread regulatory roles. Mol. Cell. Proteomics 10, M111.013284.

44. Jachimowicz RD, Beleggia F, Isensee J, Velpula BB, Goergens J, Bustos MA, Doll MA, Shenoy A, Checa-Rodriguez C, Wiederstein JL, et al. (2019). UBQLN4 represses homologous recombination and is overexpressed in aggressive tumors. Cell 176, 505–519.e22. [PubMed: 30612738]

45. Sakthivel KM, and Hariharan S (2017). Regulatory players of DNA damage repair mechanisms: role in Cancer Chemoresistance. Biomed. Pharmacother. 93, 1238–1245. [PubMed: 28738540]

46. Qu J, Sun Z, Peng C, Li D, Yan W, Xu Z, Hou Y, Shen S, Chen P, and Wang T (2021). C. tropicalis promotes chemotherapy resistance in colon cancer through increasing lactate production to regulate the mismatch repair system. Int. J. Biol. Sci. 17, 2756–2769.

47. Shi T, Ma Y, Cao L, Zhan S, Xu Y, Fu F, Liu C, Zhang G, Wang Z, Wang R, et al. (2019). B7-H3 promotes aerobic glycolysis and chemoresistance in colorectal cancer cells by regulating HK2. Cell Death Dis. 10, 308. [PubMed: 30952834]

48. Zhu F-Y, Wang L-L, Meng T-G, Wang R-L, Yang Z-X, Cao Y, Zhu G-Y, Jin Z, Gao L-L, Zeng W-T, et al. (2021). Inhibiting bridge integrator 2 phosphorylation leads to improved oocyte quality,

ovarian health and fertility in aging and after chemotherapy in mice. Nat. Aging 1, 1010–1023. [PubMed: 37118338]

49. Yao H, Lan J, Li C, Shi H, Brosseau JP, Wang H, Lu H, Fang C, Zhang Y, Liang L, et al. (2019). Inhibiting PD-L1 palmitoylation enhances T-cell immune responses against tumours. Nat. Biomed. Eng. 3, 306–317. [PubMed: 30952982]
50. Nasrollahi SA, Taghibiglou C, Azizi E, and Farboud ES (2012). Cell-penetrating peptides as a novel transdermal drug delivery system. Chem. Biol. Drug Des. 80, 639–646. [PubMed: 22846609]
51. Koren E, Apte A, Sawant RR, Grunwald J, and Torchilin VP (2011). Cell-penetrating TAT peptide in drug delivery systems: proteolytic stability requirements. Drug Deliv. 18, 377–384. [PubMed: 21438724]
52. Li K, Zhang TT, Zhao CX, Wang F, Cui B, Yang ZN, Lv XX, Yeerjiang Z, Yuan YF, Yu JM, et al. (2021). Faciogenital dysplasia 5 supports cancer stem cell traits in basal-like breast cancer by enhancing EGFR stability. Sci. Transl. Med. 13, eabb2914.
53. Liberti MV, and Locasale JW (2016). The Warburg effect: how does it benefit cancer cells? Trends Biochem. Sci. 41, 211–218. [PubMed: 26778478]
54. Chakraborty PK, Mustafi SB, Xiong X, Dwivedi SKD, Nesin V, Saha S, Zhang M, Dhanasekaran D, Jayaraman M, Mannel R, et al. (2017). MICU1 drives glycolysis and chemoresistance in ovarian cancer. Nat. Commun. 8, 14634. [PubMed: 28530221]
55. Soni VK, Shukla D, Kumar A, and Vishvakarma NK (2020). Curcumin circumvent lactate-induced chemoresistance in hepatic cancer cells through modulation of hydroxycarboxylic acid receptor-1. Int. J. Biochem. Cell Biol. 123, 105752.
56. Sung P, and Klein H (2006). Mechanism of homologous recombination: mediators and helicases take on regulatory functions. Nat. Rev. Mol. Cell Biol. 7, 739–750. [PubMed: 16926856]
57. Trenner A, and Sartori AA (2019). Harnessing DNA double-strand break repair for cancer treatment. Front. Oncol. 9, 1388. [PubMed: 31921645]
58. Qi Z, Redding S, Lee JY, Gibb B, Kwon Y, Niu H, Gaines WA, Sung P, and Greene EC (2015). DNA sequence alignment by microhomology sampling during homologous recombination. Cell 160, 856–869. [PubMed: 25684365]
59. Stracker TH, and Petrini JH (2011). The MRE11 complex: starting from the ends. Nat. Rev. Mol. Cell Biol. 12, 90–103. [PubMed: 21252998]
60. Mimitou EP, and Symington LS (2008). Sae2, Exo1 and Sgs1 collaborate in DNA double-strand break processing. Nature 455, 770–774. [PubMed: 18806779]
61. Nimonkar AV, Genschel J, Kinoshita E, Polaczek P, Campbell JL, Wyman C, Modrich P, and Kowalczykowski SC (2011). BLM-DNA2-RPA-MRN and EXO1-BLM-RPA-MRN constitute two DNA end resection machineries for human DNA break repair. Genes Dev. 25, 350–362. [PubMed: 21325134]
62. Giannini G, Ristori E, Cerignoli F, Rinaldi C, Zani M, Viel A, Ottini L, Crescenzi M, Martinotti S, Bignami M, et al. (2002). Human MRE11 is inactivated in mismatch repair-deficient cancers. EMBO Rep. 3, 248–254. [PubMed: 11850399]
63. Lu R, Zhang H, Jiang YN, Wang ZQ, Sun L, and Zhou ZW (2021). Post-translational modification of MRE11: its implication in DDR and diseases. Genes (Basel) 12, 1158. [PubMed: 34440334]
64. Wang Z, Gong Y, Peng B, Shi R, Fan D, Zhao H, Zhu M, Zhang H, Lou Z, Zhou J, et al. (2019). MRE11 UFMylation promotes ATM activation. Nucleic Acids Res. 47, 4124–4135. [PubMed: 30783677]
65. Li Z, Li J, Kong Y, Yan S, Ahmad N, and Liu X (2017). Plk1 phosphorylation of Mre11 antagonizes the DNA damage response. Cancer Res. 77, 3169–3180. [PubMed: 28512243]
66. Boisvert FM, Déry U, Masson JY, and Richard S (2005). Arginine methylation of MRE11 by PRMT1 is required for DNA damage checkpoint control. Genes Dev. 19, 671–676. [PubMed: 15741314]
67. Bai Y, Wang W, Li S, Zhan J, Li H, Zhao M, Zhou XA, Li S, Li X, Huo Y, et al. (2019). C1QBP promotes homologous recombination by stabilizing MRE11 and controlling the assembly and activation of MRE11/RAD50/NBS1 complex. Mol. Cell 75, 1299–1314.e6. [PubMed: 31353207]

68. He YJ, Meghani K, Caron MC, Yang C, Ronato DA, Bian J, Sharma A, Moore J, Niraj J, Detappe A, et al. (2018). DYNLL1 binds to MRE11 to limit DNA end resection in BRCA1-deficient cells. Nature 563, 522–526. [PubMed: 30464262]

69. Mojumdar A, Sorenson K, Hohl M, Toulouze M, Lees-Miller SP, Dubrana K, Petrini JHJ, and Cobb JA (2019). Nej1 interacts with Mre11 to regulate tethering and Dna2 binding at DNA double-strand breaks. Cell Rep. 28, 1564–1573.e3. [PubMed: 31390569]

70. Iacovoni JS, Caron P, Lassadi I, Nicolas E, Massip L, Trouche D, and Legube G (2010). High-resolution profiling of gammaH2AX around DNA double strand breaks in the mammalian genome. EMBO J. 29, 1446–1457. [PubMed: 20360682]

71. Zhou Y, Caron P, Legube G, and Paull TT (2014). Quantitation of DNA double-strand break resection intermediates in human cells. Nucleic Acids Res. 42, e19. [PubMed: 24362840]

72. Knijnenburg TA, Wang L, Zimmermann MT, Chambwe N, Gao GF, Cherniack AD, Fan H, Shen H, Way GP, Greene CS, et al. (2018). Genomic and molecular landscape of DNA damage repair deficiency across the cancer genome atlas. Cell Rep. 23, 239–254.e6. [PubMed: 29617664]

73. Telli ML, Timms KM, Reid J, Hennessy B, Mills GB, Jensen KC, Szallasi Z, Barry WT, Winer EP, Tung NM, et al. (2016). Homologous recombination deficiency (HRD) score predicts response to platinum-containing neoadjuvant chemotherapy in patients with triple-negative breast cancer. Clin. Cancer Res. 22, 3764–3773. [PubMed: 26957554]

74. Goldman M, Craft B, Hastie M, Repečka K, McDade F, Kamath A, Banerjee A, Luo Y, Rogers D, Brooks AN, et al. (2019). The UCSC Xena platform for public and private cancer genomics data visualization and interpretation. Preprint at bioRxiv.

Highlights

- MRE11 is lactylated by CBP in response to DNA damage and dependent on ATM
- Lactylation of MRE11 promotes DNA end resection and HR repair
- High-lactate levels in cancer cells lead to MRE11 lactylation and chemoresistance
- Inhibiting MRE11 lactylation sensitizes cancer cells to chemotherapy

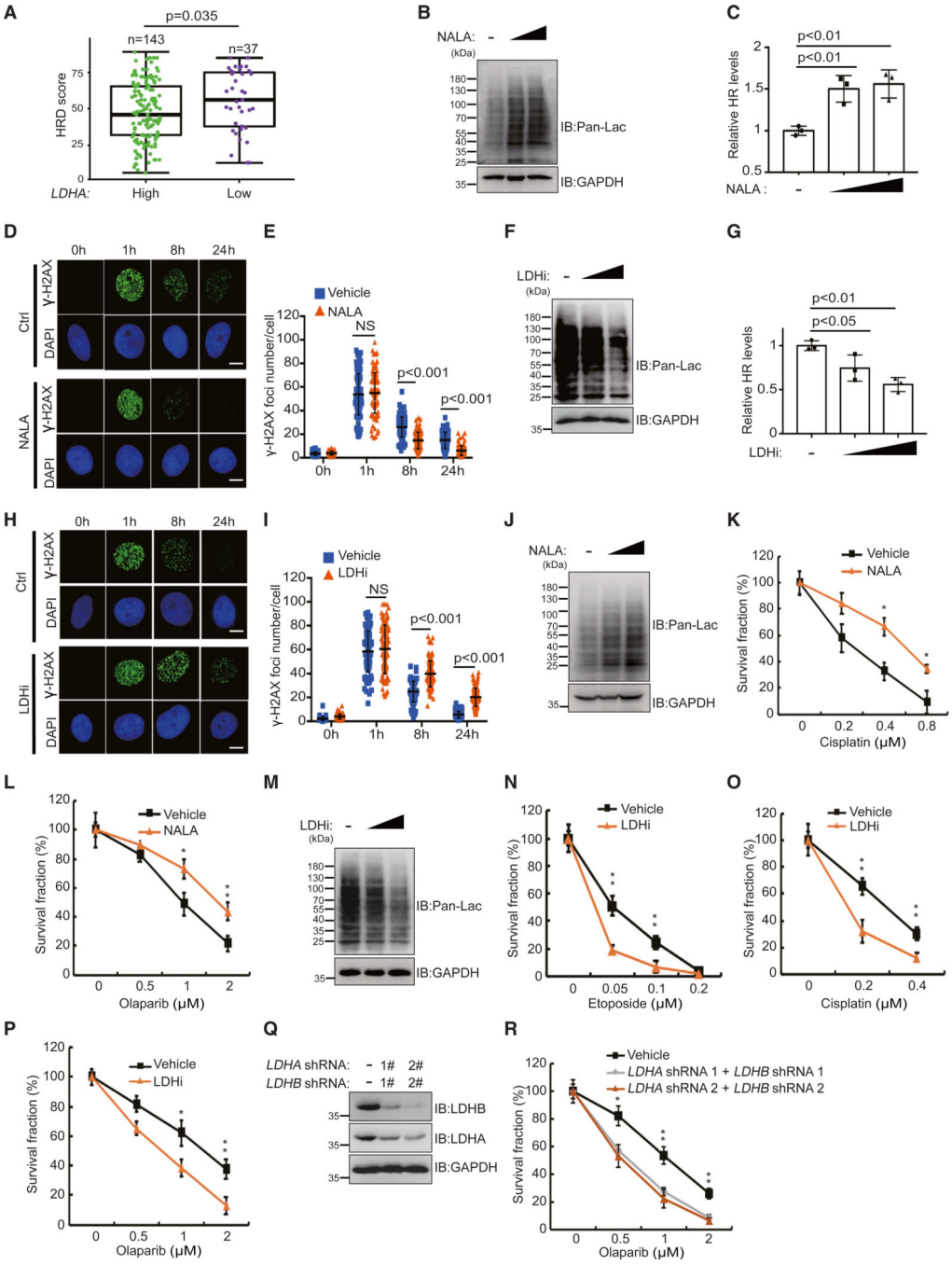

Figure 1. Lactylation plays a key role in DNA repair

(A) Analysis of HRD score in basal-like breast cancer samples. Statistical significance was tested using two-sided Mann-Whitney-Wilcoxon tests.

(B) Western blots of HEK293T cells as indicated.

(C) The HR levels of the indicated HEK293T cells were detected by fluorescence-activated cell sorting (FACS).

(D) Representative picture of γ-H2AX foci in U2OS cells treated with as indicated. Scale bars, 10 μm.

(E) Quantification of the data in (D).
(F) Western blots of samples as indicated.
(G) The HR levels of the indicated HEK293T cells were detected by FACS.
(H) Representative picture of γ-H2AX foci in U2OS cells treated with as indicated. Scale bars, 10 μm.
(I) Quantification of the data in (H).
(J) Western blots of OVCAR-8 cells treated with sodium lactate (NALA) for 24 h.
(K and L) OVCAR-8 (K) or MDA-MB-231 cells (L) were utilized for colony formation assays as indicated.
(M) Western blots of OVCAR-8 cells treated with LDHi (10 or 20 mM) for 24 h.
(N–P) OVCAR-8 (N and O) or MDA-MB-231 cells (P) were utilized for colony formation assays as indicated.
(Q) Western blots of MDA-MB-231 cells as indicated.
(R) Cells from (Q) were utilized to perform colony formation as indicated. Statistical analyses were performed with the Student's t test. *$p < 0.05$; **$p < 0.01$, NS stands for no significant change.
See also Figure S1.

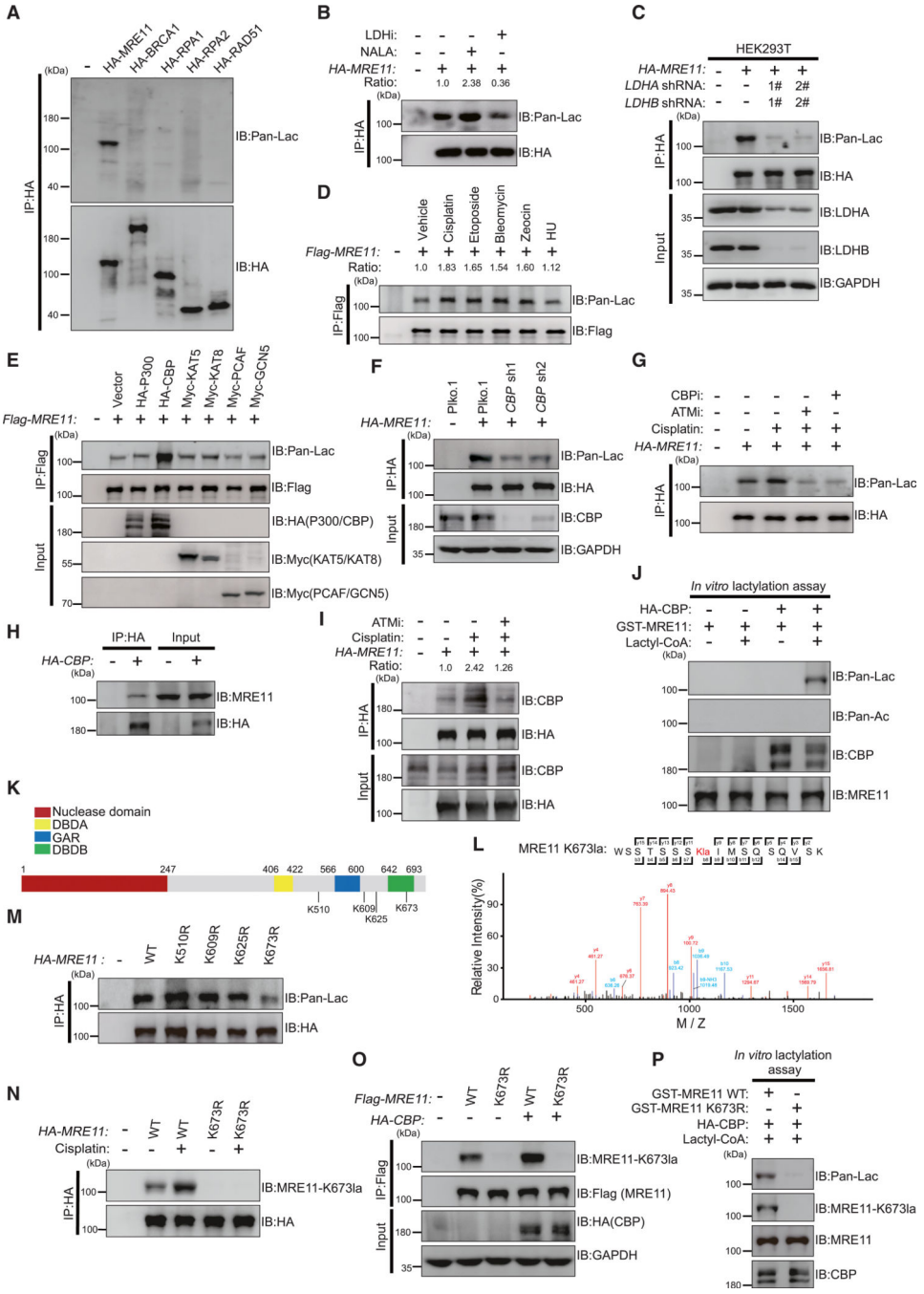

Figure 2. MRE11 K673 is lactylated by CBP

(A) Detecting lactylation of several proteins by western blots using co-immunoprecipitation (coIP) sample as indicated.

(B–D) Detecting lactylation of MRE11 in cells treated with NALA or LDHi (B), depleted *LDHA/B* (C), or treated with several inducing DNA damage chemicals (D) as indicated by western blot.

(E) Screening the “writer(s)” of MRE11 lactylation by transfecting combined MRE11 and acetyltransferase as indicated.

(F and G) Detecting lactylation of MRE11 in cells depleted *CBP* (F) or treated with chemicals as indicated by western blot. Plko.1 is a lentivirus plasmid empty vector.
(H and I) CoIP showing interactions between CBP and MRE11.
(J) Detecting MRE11 lactylation using an *in vitro* lactylation assay on the indicated samples.
(K) Schematic depicting MRE11 key domains and several lysine sites which were identified to be possibly lactylated by MS were pointed out.
(L) Illustration of MRE11 K673 lactylation identified by MS.
(M–O) Detecting lactylation of MRE11 by western blots as indicated.
(P) Detecting MRE11 lactylation using as indicated an *in vitro* lactylation assay on the indicated. Quantifications of western blots in (B), (D), and (I) using Image J software.
See also Figure S2.

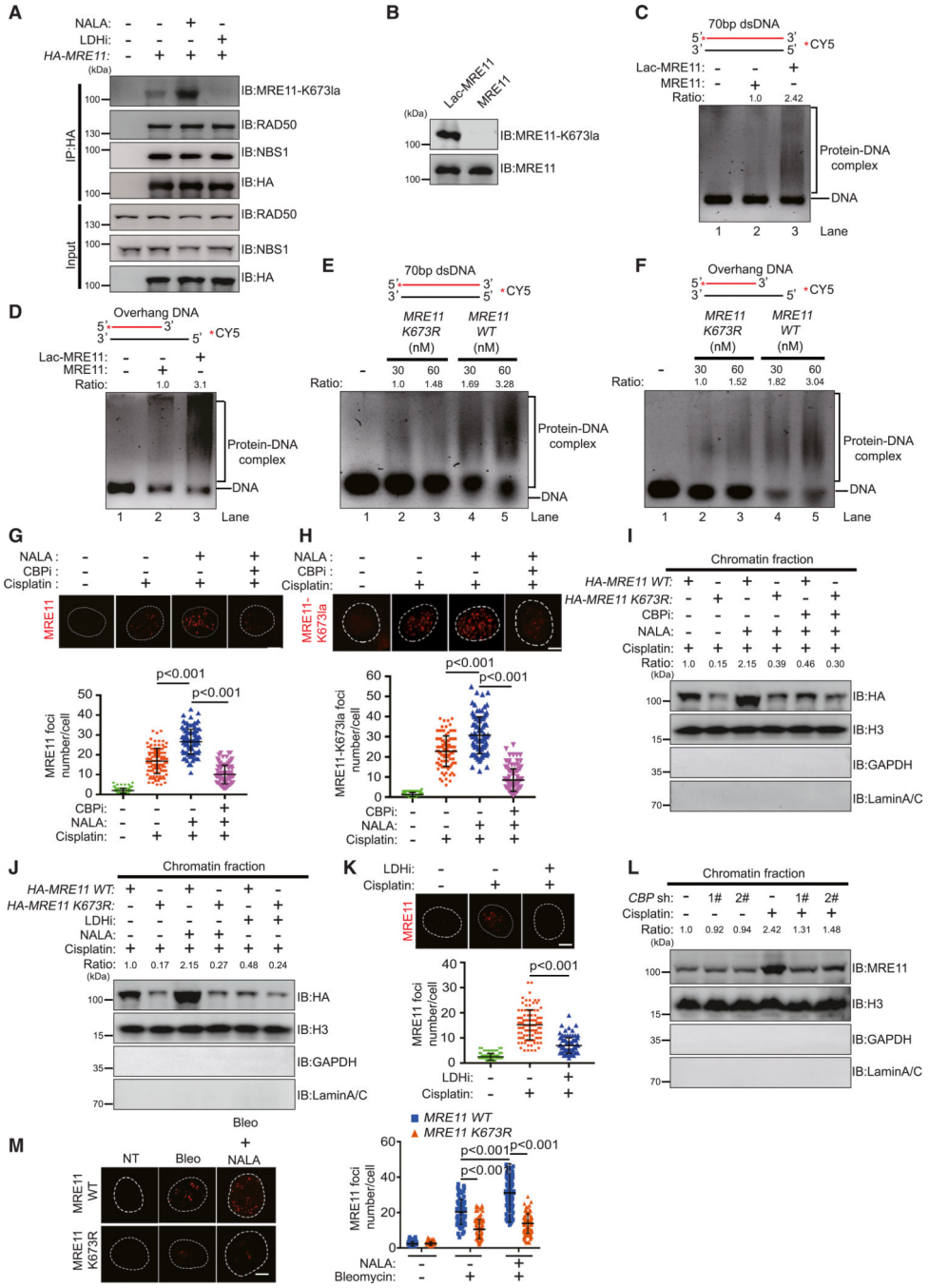

Figure 3. Lactylation of MRE11 enhances its DNA binding

(A) Western blots of as indicated coIP and input samples.

(B) MRE11 proteins were lactylated *in vitro*.

(C and D) Lactylated MRE11 proteins or unlactylated MRE11 proteins from (B) were used to perform an EMSA as indicated.

(E and F) MRE11 WT and MRE11 K673R proteins were used to perform an EMSA as indicated.

(G and H) Representative picture of MRE11(G) or MRE11-K673la (H) foci in U2OS cells as indicated treatment in upper panel. Scale bars, 10 μm. The lower panel is quantification.
(I and J) Western blots of chromatin fraction from the indicated cells.
(K) Representative picture of MRE11 foci in U2OS cells as indicated treatment in upper panel. Scale bars, 10 μm. The lower panel is quantification.
(L) Western blots of chromatin fraction from the indicated cells.
(M) Representative pictures of MRE11 foci were shown in left panel. Scale bars, 10 μm. The right panel is quantification. Quantifications of western blot or gels in (C)–(F), (I), (J), and (L) by Image J software. Statistical analyses were performed with the Student's t test. *$p < 0.05$; **$p < 0.01$; ***$p < 0.001$; NS stands for no significant change.
See also Figure S3.

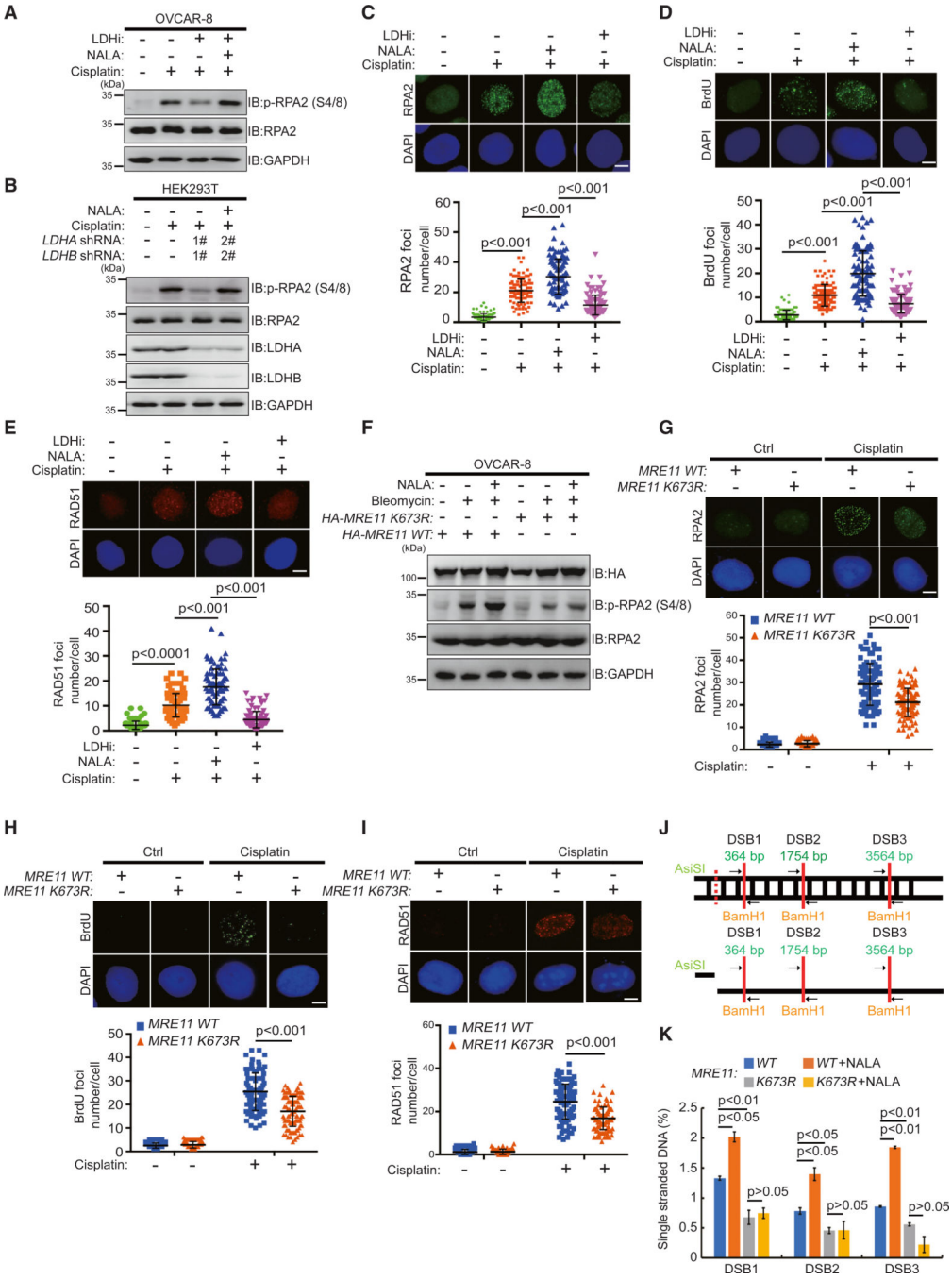

Figure 4. MRE11 lactylation promotes DNA resection

(A and B) Western blots of samples from cells treated with NALA, LDHi, and/or cisplatin for 24 h (A) or, depleted *LDHA/B* and/or cisplatin for 24 h (B) as indicated.

(C–E) Representative pictures of RPA2 (C), BrdU (D), and RAD51 (E) foci in U2OS cells with the indicated treatment are shown in upper panel. Scale bars, 10 μm. The lower panel is quantification.

(F) Western blots of the carried *MRE11 WT* or *MRE11 K673R* OVCAR-8 cells treated with NALA and/or bleomycin for 24 h as indicated.

(G–I) Representative picture of RPA2 (G), BrdU (H), and RAD51 (I) foci in as indicated U2OS cells in upper panel. Scale bars, 10 μm. The lower panel is quantification.
(J) The diagram of AsiSI-ER U2OS system for detecting single-strand DNA generated by DNA end resection.
(K) Detecting DNA end resection by qPCR using AsiSI-ER U2OS system. Statistical analyses were performed with the Student's t test. *$p < 0.05$; **$p < 0.01$; ***$p < 0.001$; NS stands for no significant change.
See also Figures S3 and S4.

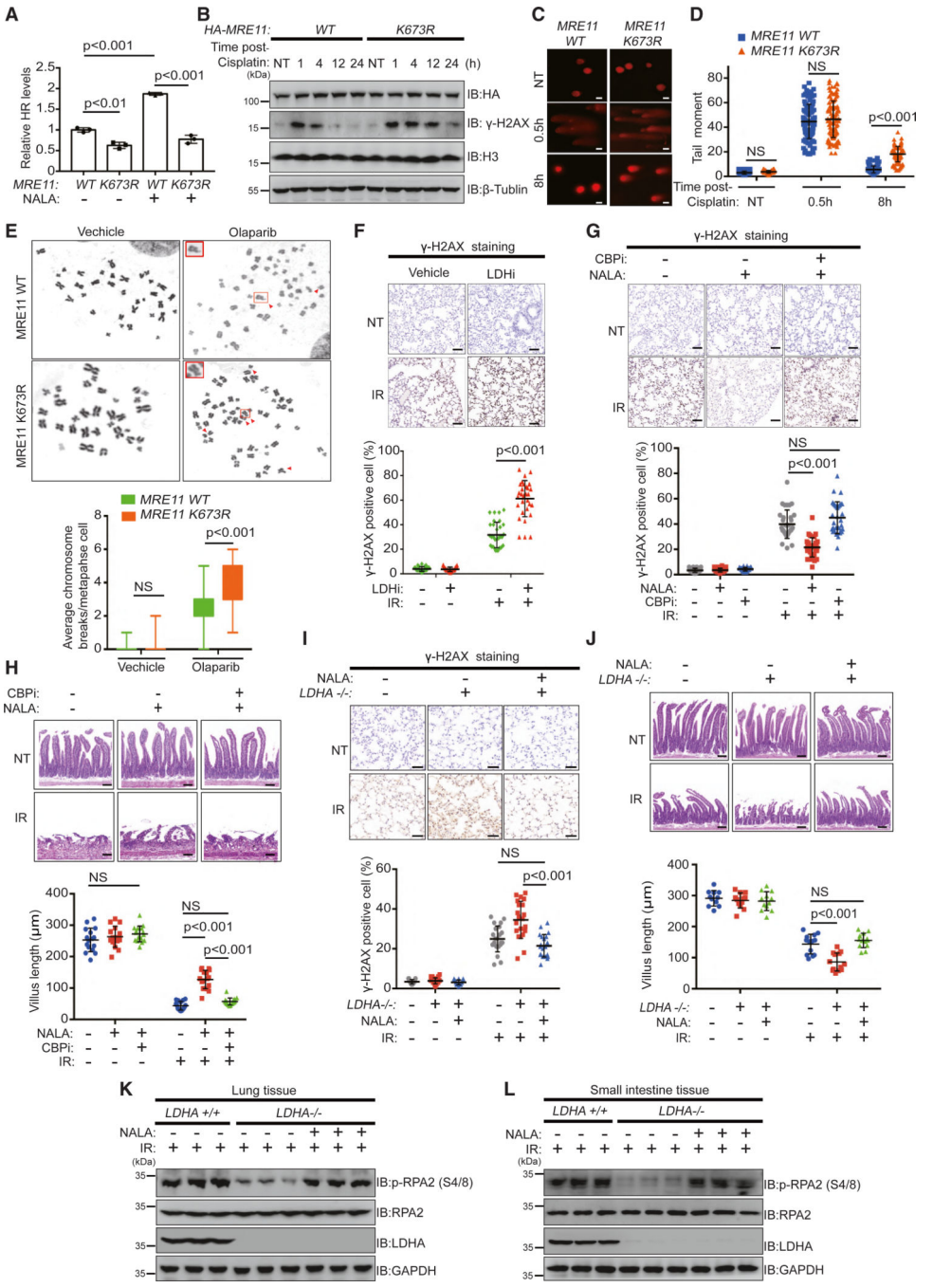

Figure 5. Inhibition of MRE11 lactylation impairs DNA damage repair

(A) The HR levels of the carried *MRE11 WT* or *MRE11 K673R* HEK293T cells treated with/without NALA for 24 h as indicated were detected by FACS.

(B) Western blots of the carried *MRE11 WT* or *MRE11 K673R* HEK293T cells treated with as indicated.

(C) Representative pictures of comet assays as indicated. Scale bars, 10 μm.

(D) Quantification of the data in (C).

(E) Genomic instability was examined by metaphase spread assays as indicated.

(F and G) Representative pictures of γ-H2AX staining in as indicated lung sections of mice (5 mice/group). Scale bars, 100 μm.

(H) Representative pictures of intestinal regenerating villi of the indicated mice. Scale bars, 50 μm.

(I) Representative pictures of γ-H2AX staining in as indicated lung sections of the indicated mice (5 mice/group). Scale bars, 100 μm.

(J) Representative pictures of intestinal regenerating villi of as indicated mice. Scale bars, 50 μm.

(K and L) Western blots of samples the indicated. Statistical analyses were performed with the Student's t test. *$p < 0.05$; **$p < 0.01$; ***$p < 0.001$; NS stands for no significant change.

See also Figure S5.

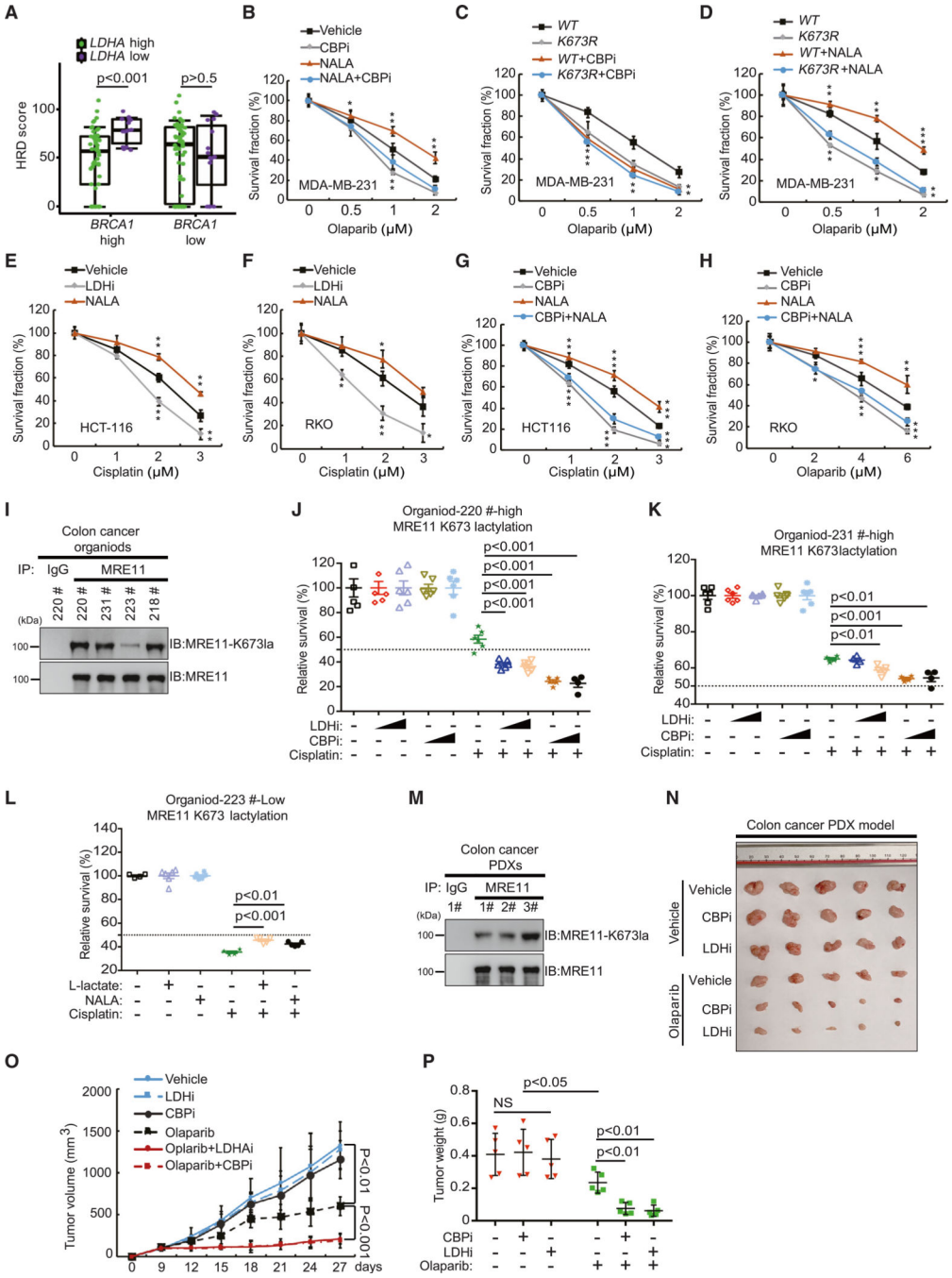

Figure 6. Inhibition of MRE11 lactylation sensitizes cancer cell to chemotherapy

(A) Analysis of HRD score in basal-like breast cancer samples. n = 140 samples. Statistical significance was tested using two-sided Mann-Whitney-Wilcoxon tests.

(B–H) Colony formation assays were performed as indicated.

(I) Western blots of four colon cancer patient-derived organoids (PDOs) as indicated.

(J and K) As indicated, two PDOs with high lactylation of MRE11 K673 were employed to perform growth assays with CCK-8 (cell counting kit-8) assays.

(L) PDO 223 with low lactylation of MRE11 K673 was employed to perform growth assays with CCK-8.
(M) Western blots of three colon cancer patients derived xenografts (PDXs), as indicated.
(N–P) Nu/Nu mice were transplanted subcutaneously with PDX from (M) and treated as indicated. Tumor images were acquired as shown in (N); tumor volumes were calculated (O); and weights (P) were measured. n = 5; data points in (O) and (P) represent mean tumor weight ± SD. Statistical analyses were performed with the Student's t test. *p < 0.05; **p < 0.01; ***p < 0.001; NS stands for no significant change.
See also Figure S6.

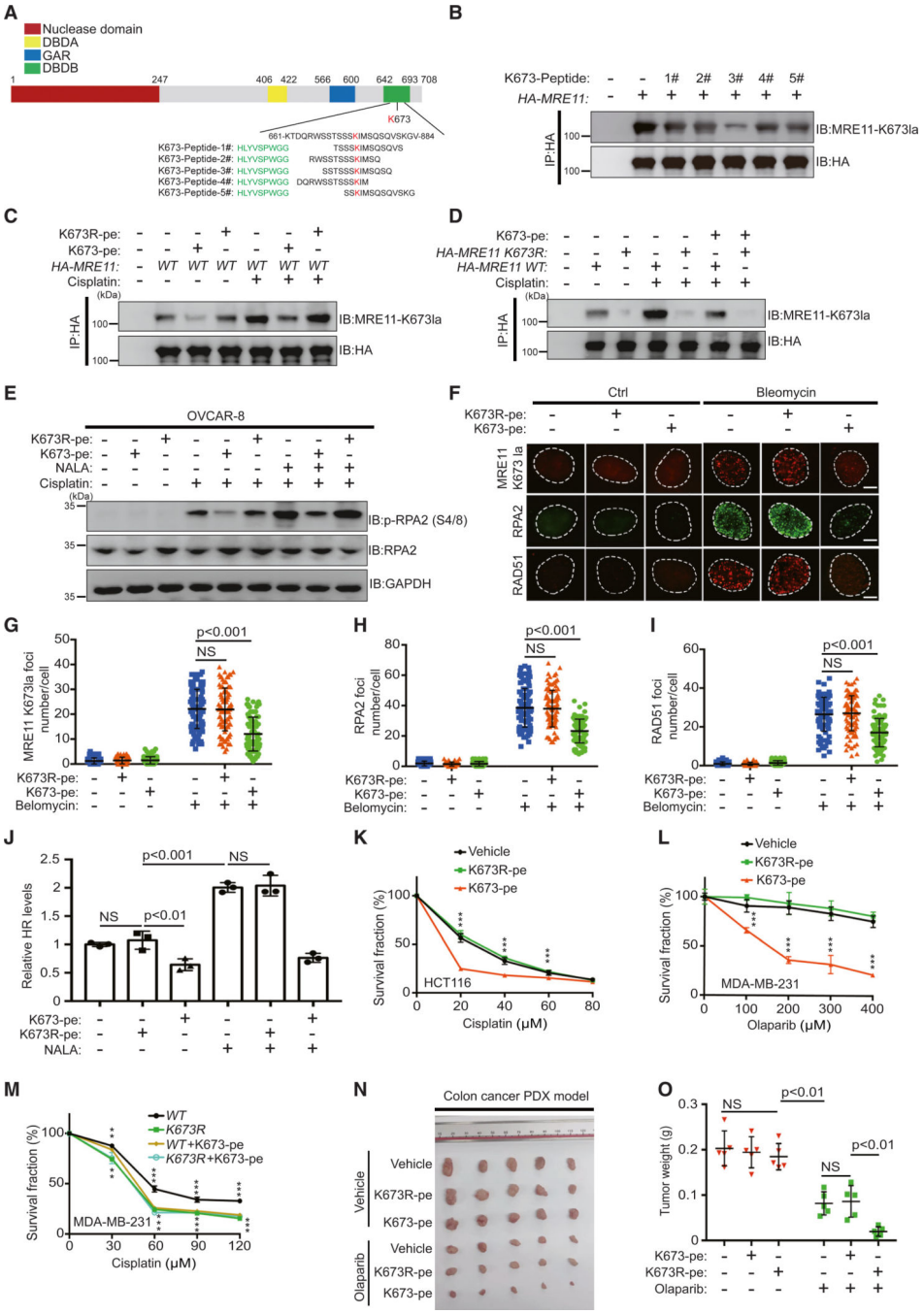

Figure 7. Targeting lactylation of MRE11 K673 via a peptidic inhibitor enhances chemotherapy sensitivity

(A) Schematic illustration of designed peptides. Green: cell-penetrating peptide (CPP). Red: site for MRE11 lactylation.

(B–E) Western blots of samples as indicated.

(F) Representative picture of MRE11 K673la, RPA2, and RAD51 foci in U2OS cells with the indicated treatment. Scale bars, 10 μm.

(G–I) Quantification of K673la (G), RPA2 (H), and RAD51 (I) foci from the data in (F).

(J) The HR levels of as indicated HEK293T cells were detected by FACS.

(K) HCT116 cells were utilized to perform CCK-8 assays as indicated.
(L) MDA-MB-231 cells were utilized to perform CCK-8 assays as indicated.
(M) As indicated MDA-MB-231 cells were utilized to perform CCK-8 assays.
(N and O) Nu/Nu mice were transplanted subcutaneously with PDX from Figure 6M and treated as indicated. Tumor images were acquired as shown in (N) and weights (O) were measured. n = 5; data points in (O) represent mean tumor weight ± SD. Statistical analyses were performed with the Student's t test. *$p < 0.05$;**$p < 0.01$; ***$p < 0.001$; NS stands for no significant change.
See also Figure S7.

KEY RESOURCES TABLE

REAGENT or RESOURCE	SOURCE	IDENTIFIER
Antibodies		
Anti-GAPDH	Proteintech	Cat# 60004–1-lg; RRID: AB_2107436
Anti-β-actin	Proteintech	Cat# 66009–1-Ig; RRID: AB_2687938
Anti-γH2AX	Millipore	Cat# 05–636; RRID: AB_309864
Anti-Flag	Sigma-Aldrich	Cat# F1804; RRID: AB_262044
Anti-HA	Cell Signaling Technology	Cat# 3724; RRID: AB_1549585
Anti-Myc	Proteintech	Cat# 16286–1-AP; RRID: AB_11182162
Anti-RPA2	Santa Cruz Biotechinology	Cat# sc-56770; RRID: AB_785534
Anti-p-S4/8-RPA2	BETHYL	Cat# A300–245; RRID: AB_210547
Anti-RAD51	Gene Tex	Cat# GTX100469; RRID: AB_1951602
Anti-BRDU	BD Biosciences	Cat# 347580; RRID: AB_400326
Anti-MRE11	Gene Tex	Cat# GTX70212; RRID: AB_372398
Anti-RAD50	Gene Tex	Cat# GTX70228; RRID: AB_372854
Anti-NBS1	Novus	Cat# NB100–143; RRID: AB_10078050
Anti-Pan-Lac	PTM Biolab	Cat# PTM-1401RM
Anti-Pan-Ac	PTM Biolab	Cat# PTM-101; RRID: AB_2940830
Anti-LDHA	Cell Signaling Technology	Cat# 2012S; RRID: AB_2137173
Anti-LDHB	Millipore	Cat# ABC927
Anti-H3	Proteintech	Cat# 17168–1-AP; RRID: AB_2716755
Anti-MRE11-K673la	PTM Biolab	N/A
Anti-MRE11-K673ac	ABclonal	N/A
Anti-Lamin A/C	Affinity Biosciences	Cat# AF6056; RRID: AB_2834975
Anti-H4	ABclonal	Cat# A23000
Anti-acetyl-H4	Active Motif	Cat# 39967; RRID: AB_2793413
Anti-acetyl-H3	Active Motif	Cat# 39140; RRID: AB_2687871
Anti-CBP	Cell Signaling Technology	Cat# 7389S; RRID: AB_2616020
Anti-GCN5	Santa Cruz Biotechinology	Cat# sc-365321
Anti-GLO1	Santa Cruz Biotechinology	Cat# sc-133144

REAGENT or RESOURCE	SOURCE	IDENTIFIER
Anti-p-S678-MRE11	Biorbyt	Cat# orb185227
Anti-p-S676-MRE11	Cell Signaling Technology	Cat# 4859S; RRID: AB_2145096
Anti-p-SQ/TQ ATM/ATR Substrate	Cell Signaling Technology	Cat# 2851; RRID: AB_330318
Anti-His	Santa Cruz Biotechinology	Cat# sc-8036; RRID: AB_627727
Anti-β-Tubulin	ABclonal	Cat# AC021; RRID: AB_2773004
Bacterial and virus strains		
DH5α	TIANGEN	Cat# CB101
BL21	TIANGEN	Cat# CB105
STBL3	Thermo Fisher Scientific	Cat# *C737303*
Chemicals, peptides, and recombinant proteins		
Cisplatin	Sigma-Aldrich	Cat# P4394
Etoposide	Sigma-Aldrich	Cat# 341205
Bleomycin	Sigma-Aldrich	Cat# 203401
Penicillin/Streptomycin	GIBCO	Cat# 15140–122
Zeocin	Thermo Fisher Scientific	Cat# R25005
Hu	Sigma-Aldrich	Cat# H8627
Sodium l-lactate	Sigma-Aldrich	Cat# 71718
L-lactic acid	Sigma-Aldrich	Cat# L1750
LDH inhibitor (Sodium oxamate)	Sigma-Aldrich	Cat# O2751
Puromycin	Sigma-Aldrich	Cat# 540222
KU55933	Sigma-Aldrich	Cat# SML1109
5-Bromo-2′-deoxyuridine (BRDU)	Sigma-Aldrich	Cat# 203806
CBP inhibitor (SGC-CBP30)	Selleckchem	Cat# S7256
PARP inhibitor (Olaparib)	Selleckchem	Cat# AZD2281
MCT1/4 inhibitor (Syrosingopine)	Selleckchem	Cat# No. S9907
GLO1 inhibitor	MedChemExpress	Cat# HY-15167A
K673-Pe	Guoping Pharmaceutic Inc	N/A
K673R-pe	Guoping Pharmaceutic Inc	N/A
Polyethylenimine (PEI)	Polysciences	Cat# 23966–100mg

REAGENT or RESOURCE	SOURCE	IDENTIFIER
Lipofectamine™ 2000	Thermo Fisher Scientific	Cat# 11668027
Lipofectamine™ 3000	Thermo Fisher Scientific	Cat# L3000150
Polybrene	Sigma-Aldrich	Cat# H9268
Tamoxifen	Sigma-Aldrich	Cat# T5648
XhoI	New England Biolabs (NEB)	Cat# R0146V
ECoRI-HF	New England Biolabs (NEB)	Cat# R3101V
BamH1	New England Biolabs (NEB)	Cat# R0136V
Micrococal nuclease	New England Biolabs (NEB)	Cat# M0247S
4-Hydroxytamoxifen (4-OHT)	Sigma-Aldrich	Cat# H6278
DTT	Sigma-Aldrich	Cat# 3483–12-3
NP-40	Sigma-Aldrich	Cat# 127087–87-0
HEPES	Sigma-Aldrich	Cat# H3662
Sodium deoxycholate	Sigma-Aldrich	Cat# 30968
Anti-HA-agarose beads	Milipore	Cat# A209
Anti-Flag-agarose beads	Milipore	Cat# A2220
Protein A/G -agarose beads	Milipore	Cat# IP10
His60 Ni Superflow Resin	Clontech	Cat# 635660
Colcemid	Sigma-Aldrich	Cat# 234109-M
Giemsa	Sigma-Aldrich	Cat# 1.09204
IPTG	Sigma-Aldrich	Cat# I6758
Microcal nuclease	New England Biolabs (NEB)	Cat# M0247S
Acetyl-CoA	Sigma-Aldrich	Cat# A2056
Lactyl-CoA	LookChem	N/A
2 x HB-infusion™ Master mix	HANBIO	N/A
Recombinant Human RAD50 protein	From Dr.Xingzhi Xu	N/A
Recombinant Human GST-MRE11 protein	This paper	N/A
Recombinant Human HA-MRE11 protein	This paper	N/A
Recombinant Human HA-CBP protein	This paper	N/A
Recombinant Human Myc-GCN5 protein	This paper	N/A
Critical commercial assays		

REAGENT or RESOURCE	SOURCE	IDENTIFIER
Genomic DNA Extraction Kit	TIANGEN	Cat# DP304
Plasmid Extraction Kit	TIANGEN	Cat# DP103
Taqman Universal PCR Master Mix	Applied Biosystems™	Cat# 4304437
Lactate Colorimetric/Fluorometric assay kit	Abcam	Cat# ab65331
PrimeScript™ RT reagent Kit with gDNA Eraser (Perfect Real Time)	TAKARA	Cat# RR047A
PrimeSTAR® GXL DNA Polymerase	TAKARA	Cat# R050A
PowerUp™ SYBR™ Green	Applied Biosystems™	Cat# A25743
CCK8 kit	KeyGEN BioTECH	Cat# KGA317
Experimental models: Cell lines		
Human: U2OS cells	ATCC	Cat# HTB-96
Human: HEK-293T cells	ATCC	Cat# CRL-3216
Human: HCT116 cells	ATCC	Cat# CCL-247
Human: MD-MBA-231 cells	ATCC	Cat# CRM-HTB-26
Experimental models: Organisms/strains		
Mouse: UBC-Cre^{ERT}-LDHA $^{fl/fl}$: C57BL/6N	This paper	N/A
Mouse: C57BL/6N	Charles River	Strain# 213
Mouse: BALB/*c* Nude	Charles River	Strain# 401
Oligonucleotides		
See Table S1	N/A	N/A
Recombinant DNA		
pLVX3-puro-Flag-HA-MRE11 WT	This paper	N/A
pLVX3-puro-Flag-HA-MRE11 K673R	This paper	N/A
pLVX3-puro-Flag-HA-MRE11 K161R	This paper	N/A
pLVX3-puro-Flag-HA-MRE11 K384R	This paper	N/A
pLVX3-puro-Flag-HA-MRE11 K393R	This paper	N/A
pLVX3-puro-Flag-HA-MRE11 K407R	This paper	N/A
pLVX3-puro-Flag-HA-MRE11 K480R	This paper	N/A

REAGENT or RESOURCE	SOURCE	IDENTIFIER
pLVX3-puro-Flag-HA-MRE11 K510R	This paper	N/A
pLVX3-puro-Flag-HA-MRE11 K609R	This paper	N/A
pLVX3-puro-Flag-HA-MRE11 K625R	This paper	N/A
pLVX-puro-Flag-MRE11 WT	This paper	N/A
pLVX-puro-Flag-MRE11 K673R	This paper	N/A
pLVX-puro-HA-MRE11 K673R	This paper	N/A
pLVX-puro-HA-MRE11 WT	This paper	N/A
pEGX-4T-2-MRE11 WT	This paper	N/A
pEGX-4T-2-MRE11 K673R	This paper	N/A
pEGX-4T-2-MRE11 K609R	This paper	N/A
Software and algorithms		
Image J 1.8.0	NIH	N/A
GraphPad Prism 7	GraphPad Software	Version 6
Adobe Illustrator CS6	Adobe	N/A